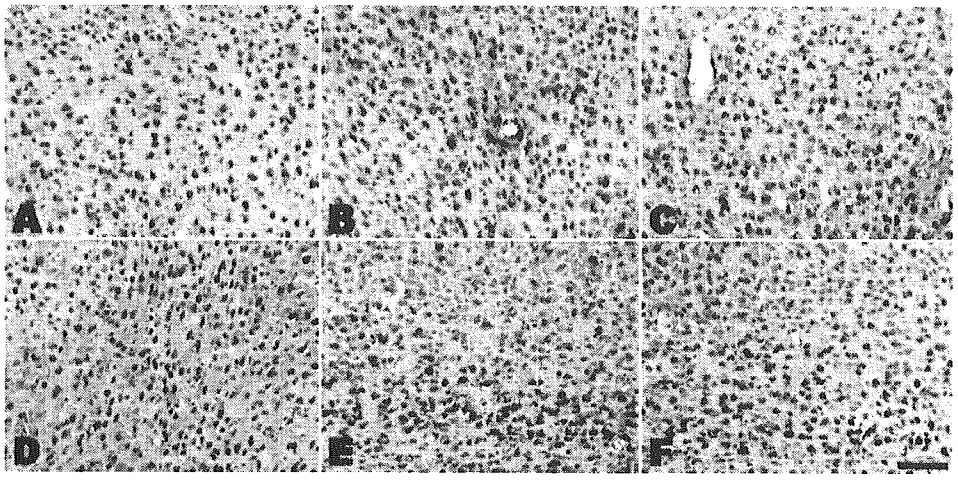

Fig. 4. Distinct localizations of SP immunoreactive (ir) cells in the frontal cortex area 1 (A, B, C) and occipital cortex area 1 of 4-week-old NPC $^{(-/-)}$ (C, F), NPC $^{(+/-)}$ (B, E), and NPC $^{(+/+)}$ (A, D) mouse. In all three types of mice, SP-ir cells were present prominently in the IV–VI layers. Interestingly, SP-ir cells in the 4-week-old NPC $^{(+/+)}$ occipital cortex 1 (D) had long and prominent processes. Scale bar = 100 μm.

levels in the cerebral cortex of the AD brain. Although no report is available concerning the distribution of NPY-ir cells in the cerebral cortex of NPC mouse. Several have described age-related changes of NPY-ir cells in the rat cerebral cortex. Cha et al. [4] reported 10–50% reductions in NPY-ir neurons in the cerebral cortices of aged rats, and Zoli et al. [29] reported a 50% reduction in NPY-ir neuron count in the aged rat neostriatum. These discrepancies concerning VIP and NPY may be due to different pathogeneses, species, or the experimental methods used, as has been found in many other neurotransmitter systems.

SP, a representative of the tachykinin peptide family, is the first bioactive peptide derived from neural tissue [13] and has many known functions (e.g., pain transmission, and the control of the respiratory and cardiovascular systems). SP-ir cells have been shown to be widely distributed in the CNS [16]. In the monkey, many SP-ir cell bodies and fibers were observed in layers II–VI throughout the cerebral cortex, and the majority of these cells had bipolar or multipolar morphologies [10]. In line with our data, a previous study in the rat also found that SP-ir cells [as revealed by another SP antibody (Biogenesis, Cat. No. AR1768)] were scattered throughout the cerebral cortex, and the number of SP-ir cells were 386–545 in the rat cerebral cortex [25]. SP may also be associated with neurodegenerative disease: AD and Huntington's disease [13]. An examination of SP distribution in the AD isocortex and allocortex, using a monoclonal anti-SP antibody, showed SP depletion in AD [13]. SP-IR was also found to be significantly attenuated in the cerebral cortex of Rett syndrome, a motor disability disease that occurs in women [5]. In the present study, we did not find any statistically significant ($P < 0.05$) differences between the SP-ir cell number staining with 20064 and MAB 356 SP antibody. Major differences were found between NPC $^{(+/-)}$ and NPC $^{(+/+)}$, and between NPC $^{(-/-)}$ and NPC $^{(+/+)}$ in all three regions of the frontal and parietal 1 cortex. The reasons for these regional variations between the NPC $^{(+/-)}$ versus NPC $^{(+/+)}$ are not determinable by this morphological study alone.

German et al. suggested that all neurons are not equally vulnerable to degeneration in NPC $^{(-/-)}$ mouse. At 11 weeks of age, low levels of neuron loss were evident in the thalamus and prefrontal cortex of NPC $^{(-/-)}$ mouse, though they show a 96% loss of Purkinje cells in the cerebellum [8]. Thus, in NPC $^{(-/-)}$ mouse, specific neurons are targeted by disease whereas other neurons are less vulnerable to degeneration. In the 3-week-old NPC $^{(-/-)}$ mouse, there was an age-related reduction in the number of neurons in the prefrontal cortex (28% reductions) and thalamus (20% reductions) [8]. However, in this study, no substantial cell losses were found in any cortex area of the 4-week-, 11-week-old NPC $^{(-/-)}$ mouse versus age-matched NPC $^{(+/+)}$ or NPC $^{(+/-)}$ mouse by cresyl-violet staining (Figs. 1D–F). This may indicate that no massive degeneration or apoptosis occurred to the NPC $^{(-/-)}$ mouse cortex by 11 weeks of age. Therefore, given the fundamental role of NPC1 in intracellular lipid transport, we suggest that abnormal lipid accumulation may be the primary defect in NPC and that this leads to secondary neurological impairment [23]. Previous studies demonstrated that the increased cellular accumulation of lysosomes causes an increase in lysosomal hydrolases (e.g., cathepsin-D), which can have a toxic effect on cells [19,26]. The levels of cathepsins D and E were significantly increased during normal aging process [18]. In the NPC model mouse, age-related elevations in cathepsin-D have been observed in both neurons and microglial cells [9]. Microglial activation is also needed by the neurodegenerative process of another lysosomal storage disease, Sandhoff disease [26]. Cathepsin-E hydrolyzed tachykinins, such as substance P and neurokinin A, with specific cleavage of essential sequences for their activity [11]. Thus, the reduced numbers of SP-ir cells in NPC $^{(-/-)}$ mouse appear not to represent a developmental abnormality, but rather appear to be related with an abnormal

lysosomal metabolism. However, based on the results of the present study in isolation, it is not possible to determine whether reduced SP-ir cell numbers are directly related to the etiology of this disease. Overall, these results suggest that the neuropathological consequences of NPC are highly influenced by the neurotransmitter system, especially, SP, in the cerebral cortex.

The present study demonstrates significantly reduced SP-ir cell numbers in the cerebral cortex of 11-week-old NPC $^{(-/-)}$ mouse, which suggests that a pathway rather than one involving NPC1 protein itself may be responsible for the disease consequences observed in the NPC $^{(-/-)}$ mouse cerebral cortex. We hope that our study provides useful data for future investigations.

Acknowledgment

This work was supported in part by the National Niemann–Pick Disease Foundation, Inc., USA.

References

[1] S. Akaboshi, T. Yano, S. Miyawaki, K. Ohno, K.A. Takeshita, C57BL/KsJ mouse model of Niemann–Pick disease (spm) belongs to the same complementation group as the major childhood type of Niemann–Pick disease type C, Hum. Genet. 99 (1997) 350–353.

[2] H. Arai, T. Moroji, K. Kosaka, Somatostatin and vasoactive intestinal polypeptide in postmortem brains from patients with Alzheimer-type dementia, Neurosci. Lett. 52 (1984) 73–78.

[3] E.D. Carstea, J.A. Morris, K.G. Coleman, S.K. Loftus, D. Zhang, C. Cummings, J. Gu, M.A. Rosenfeld, W.J. Pavan, D.B. Krizman, J. Nagle, M.H. Polymeropoulos, S.L. Sturley, Y.A. Ioannou, M.E. Higgins, M. Comly, A. Cooney, A. Brown, C.R. Kaneski, E.J. Blanchette-Mackie, N.K. Dwyer, E.B. Neufeld, T.Y. Chang, L. Liscum, D.A. Tagle, et al., Niemann–Pick C1 disease gene: homology to mediators of cholesterol homeostasis, Science 277 (1997) 228–231.

[4] C.I. Cha, Y.I. Lee, E.Y. Lee, K.H. Park, S.H. Baik, Age-related changes of VIP, NPY and somatostatin-immunoreactive neurons in the cerebral cortex of aged rats, Brain Res. 753 (1997) 235–244.

[5] K. Deguchi, B.A. Antalffy, L.J. Twohill, S. Chakraborty, D.G. Glaze, D.D. Armstrong, Substance P immunoreactivity in Rett syndrome, Pediatr. Neurol. 22 (2000) 259–266.

[6] R.P. Erickson, O. Bernard, Studies on neuronal death in the mouse model of Niemann–Pick C disease, J. Neurosci. Res. 68 (2002) 738–744.

[7] N.L. Foster, C.A. Tamminga, T.L. O'Donohue, K. Tanimoto, E.D. Bird, T.N. Chase, Brain choline acetyltransferase activity and neuropeptide Y concentrations in Alzheimer's disease, Neurosci. Lett. 63 (1986) 71–75.

[8] D.C. German, E.M. Quintero, C.L. Liang, B. Ng, S. Punia, C. Xie, J.M. Dietschy, Selective neurodegeneration, without neurofibrillary tangles, in a mouse model of Niemann–Pick C disease, J. Comp. Neurol. 433 (2001) 415–425.

[9] D.C. German, C.-L. Liang, T. Song, U. Yazdani, C. Xie, J.M. Dietschy, Neurodegeneration in the Niemann–Pick C mouse: glial involvement, Neuroscience 109 (2002) 437–450.

[10] S. Iritani, M. Fujii, K. Satoh, The distribution of substance P in the cerebral cortex and hippocampal formation: an immunohistochemical study in the monkey and rat, Brain Res. Bull. 22 (1989) 295–303.

[11] T. Kageyama, Rabbit procathepsin E and cathepsin E. Nucleotide sequence of cDNA, hydrolytic specificity for biologically active peptides and gene expression during development, Eur. J. Biochem. 216 (1993) 717–728.

[12] D.C. Ko, M.D. Gordon, J.Y. Jin, M.P. Scott, Dynamic movements of organelles containing Niemann–Pick C1 protein: NPC1 involvement in late endocytic events, Mol. Biol. Cell 12 (2001) 601–614.

[13] N.W. Kowall, B.J. Quigley Jr., J.E. Krause, F. Lu, B.E. Kosofsky, R.J. Ferrante, Substance P and substance P receptor histochemistry in human neurodegenerative diseases, Regul. Pept. 46 (1993) 174–185.

[14] Y. Liu, Y.P. Wu, R. Wada, E.B. Neufeld, K.A. Mullin, A.C. Howard, P.G. Pentchev, M.T. Vanier, K. Suzuki, R.L. Proia, Alleviation of neuronal ganglioside storage does not improve the clinical course of the Niemann–Pick C disease mouse, Hum. Mol. Genet. 9 (2000) 1087–1092.

[15] S.K. Loftus, J.A. Morris, E.D. Carstea, J.Z. Gu, C. Cummings, A. Brown, J. Ellison, K. Ohno, M.A. Rosenfeld, D.A. Tagle, P.G. Pentchev, W.J. Pavan, Murine model of Niemann–Pick C disease: mutation in a cholesterol homeostasis gene, Science 277 (1997) 232–235.

[16] J. Marksteiner, A. Saria, R. Kirchmair, R. Pycha, H. Benesch, R. Fischer-Colbrie, C. Haring, H. Maier, G. Ransmayr, Distribution of secretoneurin-like immunoreactivity in comparison with substance P- and enkephalin-like immunoreactivities in various human forebrain regions, Eur. J. Neurosci. 5 (1993) 1573–1585.

[17] M.F. Mazurek, M.F. Beal, E.D. Bird, J.B. Martin, Vasopressin in Alzheimer's disease: a study of postmortem brain concentrations, Ann. Neurol. 20 (1986) 665–670.

[18] H. Nakanishi, Neuronal and microglial cathepsins in aging and age-related diseases, Ageing Res. Rev. 2 (2003) 367–381.

[19] K. Ohmi, D.S. Greenberg, K.S. Rajavel, S. Ryazantsev, H.H. Li, E.F. Neufeld, Activated microglia in cortex of mouse models of mucopolysaccharidoses I and IIIB, Proc. Natl. Acad. Sci. U. S. A. 100 (2003) 1902–1907.

[20] R.H. Perry, G.J. Dockray, R. Dimaline, E.K. Perry, G. Blessed, B.E. Tomlinson, Neuropeptides in Alzheimer's disease, depression and schizophrenia: a post mortem analysis of vasoactive intestinal peptide and cholecytokinin in cerebral cortex, J. Neurol. Sci. 51 (1981) 465–472.

[21] P.C. Reid, S. Sugii, T.Y. Chang, Trafficking defects in endogenously synthesized cholesterol in fibroblasts, macrophages, hepatocytes, and glial cells from Niemann–Pick type C1 mice, J. Lipid Res. 44 (2003) 1010–1019.

[22] M.T. Vanier, K. Suzuki, Recent advances in elucidating Niemann–Pick C disease, Brain Pathol. 8 (1998) 163–174.

[23] I. Vincent, B. Bu, R.P. Erickson, Understanding Niemann–Pick type C disease: a fat problem, Curr. Opin. Neurol. 16 (2003) 155–161.

[24] V. Voikar, H. Rauvala, E. Ikonen, Cognitive deficit and development of motor impairment in a mouse model of Niemann–Pick type C disease, Behav. Brain Res. 132 (2002) 1–10.

[25] M. Vruwink, H.H. Schmidt, R.J. Weinberg, A. Burette, Substance P and nitric oxide signaling in cerebral cortex: anatomical evidence for reciprocal signaling between two classes of interneurons, J. Comp. Neurol. 441 (2001) 288–301.

[26] R. Wada, C.J. Tifft, R.L. Proia, Microglial activation precedes acute neurodegeneration in Sandhoff disease and is suppressed by bone marrow transplantation, Proc. Natl. Acad. Sci. U. S. A. 97 (2000) 10954–10959.

[27] H. Weintraub, A. Abramovici, U. Sandbank, P.G. Pentchev, R.O. Brady, M. Sekine, A. Suzuki, B. Sela, Neurological mutation characterized by dysmyelination in NCTR-Balb/C mouse with lysosomal lipid storage disease, J. Neurochem. 45 (1985) 665–672.

[28] G. Yadid, I. Sotnik-Barkai, C. Tornatore, B. Baker-Cairns, J. Harvey-White, P.G. Pentchev, E. Goldin, Neurochemical alterations in the cerebellum of a murine model of Niemann–Pick type C disease, Brain Res. 799 (1998) 250–256.

[29] M. Zoli, F. Ferraguti, G. Toffano, K. Fuxe, L.F. Agnati, Neurochemical alterations but not nerve cell loss in aged rat neostriatum, J. Chem. Neuroanat. 6 (1993) 131–145.

Journal of Neuroscience Research 80:114–119 (2005)

Oligomerization of Amyloid β-Protein Occurs During the Isolation of Lipid Rafts

Wenxin Yu,[1] Kun Zou,[1] Jian-Sheng Gong,[1,2] Mihee Ko,[1] Katsuhiko Yanagisawa,[1] and Makoto Michikawa[1]*

[1]Department of Alzheimer's Disease Research, National Institute for Longevity Sciences, Aichi, Japan
[2]The Organization of Pharmaceutical Safety and Research of Japan, Tokyo, Japan

Cholesterol- and glycosphingolipid-rich microdomains, called "lipid rafts," are suggested to initiate and promote the pathophysiology of Alzheimer's disease by serving as a platform for generation, aggregation, or degradation of amyloid-β protein (Aβ). However, methods for biochemical isolation of these microdomains may produce artifacts. In this study, when synthetic Aβ1–40 monomers were added to the brain fragment at a final concentration of 2.1 μM, followed by homogenization and isolation of lipid rafts by an established method, Aβ1–40 accumulated as oligomers in the lipid raft fraction. However, in the absence of a brain homogenate, synthetic Aβ1–40 did not accumulate in the lipid raft fraction. When fractionation was performed in the absence of synthetic Aβ1–40 and synthetic Aβ1–40 was incubated in an aliquot of each fraction, a marked oligomerization of Aβ1–40 was observed in the lipid raft aliquot. These results indicate that exogenous Aβ associates with lipid rafts, and Aβ bound to rafts forms oligomers during the isolation of lipid rafts. In addition, endogenous Aβ1–40 in a Triton X-100-insoluble fraction of a brain homogenate of the Tg2576 transgenic mouse model of Alzheimer's disease formed oligomers when the fraction was incubated at 4°C for 20 hr. Thus, one should be careful when one discusses the role of lipid rafts in amyloid precursor protein processing and in the generation, aggregation, and degradation of Aβ.

Key words: lipid rafts; Aβ; oligomers; cholesterol; sphingolipids; Alzheimer's disease

Alzheimer's disease (AD) is a slowly progressive neurodegenerative disease accompanied by dementia and psychological symptoms (Alzneimer, 1907). Extracellular deposits of the amyloid-β protein (Aβ) consisting of 39–43-amino-acid peptides, the intracellular formation of neurofibrillary tangles composed of highly phosphorylated tau, and synaptic dysfunction accompanied by neurodegeneration are the major pathological findings in AD brains (Alzneimer, 1907). The mechanism underlying the initiation of the pathological process of AD is postulated to be the age-related aggregation of Aβ (Selkoe, 1994; Esiri et al., 1997). This amyloid hypothesis, that is, aggregated/fibrous Aβ initiates and promotes AD pathophysiologies that lead to the development of AD symptoms, has dominated for years in the AD research field, and extensive effort has focused on how the generation and aggregation of Aβ are modulated and on the roles of Aβ in the pathogenesis of AD. Several lines of evidence partially support this notion by showing that highly aggregated Aβ fibrils, but not Aβ monomers, induce AD pathologies in vitro and in vivo (Mattson et al., 1993; Pike et al., 1993; Lorenzo and Yankner, 1994; Estus et al., 1997; Geula et al., 1998; Gotz et al., 2001; Morishima et al., 2001). However, recent lines of evidence have shown that not highly aggregated Aβ but, rather, smaller assemblies or oligomers of Aβ have the ability to disrupt neuronal functions, leading to neurodegeneration (Lambert et al., 1998; Hartley et al., 1999; Michikawa et al., 2001; Walsh et al., 2002; Sponne et al., 2003).

It has been shown that the cellular concentrations of cholesterol and sphingolipid modulate amyloid precursor protein (APP) processing and Aβ generation (Simons et al., 1998; Kojro et al., 2001; Sawamura et al., 2004) as well as the state of tau phosphorylation, synaptic plasticity, and neurodegeneration (Fan et al., 2001; Koudinov and Koudinova, 2001; Sawamura et al., 2001). These findings highlighted the role of lipid rafts, which are microdomains of the plasma membrane and contain high concentrations of cholesterol and sphingolipids (Simons and Ikonen, 1997). Lipid rafts exist as liquid-ordered regions of the membrane that are resistant to extraction with nonionic detergents and play important roles in signal transduction, cell adhesion, and lipid/protein sorting (Sargiacomo et al., 1993; Simons and Ikonen, 1997; Bagnat et al., 2000). Recent lines of evidence have shown that lipid rafts play a critical role in APP processing and in the generation and aggregation/deposition of Aβ (Lee et al., 1998; Morishima-Kawashima and Ihara, 1998; Oshima et al., 2001; Ehehalt et al., 2003; Kawarabayashi et al., 2004). However, it has also been suggested that meth-

Contract grant sponsor: Ministry of Health, Labor and Welfare of Japan; Contract grant number: Longevity Sciences Grant H14-10; Contract grant sponsor: Pharmaceuticals and Medical Devices Agency, Japan.

*Correspondence to: Makoto Michikawa, MD, Department of Alzheimer's Disease Research, National Institute for Longevity Sciences, 36-3 Gengo, Morioka, Obu, Aichi 474-8522, Japan. E-mail: michi@nils.go.jp

Received 21 September 2004; Revised 8 November 2004; Accepted 30 December 2004

Published online 9 February 2005 in Wiley InterScience (www.interscience.wiley.com). DOI: 10.1002/jnr.20428

ods for the biochemical isolation of these microdomains produce artifacts (Harder and Simons, 1997), which limits our interpretation of results obtained by a biochemical method of isolating lipid rafts.

Here we experimentally determined whether isolation of lipid rafts affects the accumulation and aggregation of Aβ in the lipid raft fraction by using synthetic Aβ1–40. We found that the biochemical isolation of lipid rafts promotes Aβ oligomerization. These results suggest that one should be careful when interpreting the results of APP processing and Aβ metabolism in lipid rafts isolated by a classical biochemical method.

MATERIALS AND METHODS

Immunoblot Analysis

For the detection of Aβ, proteins separated by using 4–20% gradient Tris/tricine SDS-PAGE were electrophoretically transferred onto a nitrocellulose membrane. Highly sensitive immunoblotting was performed as described previously (Sudoh et al., 1998). For the detection of flotilin-1, a raft marker, and transferrin receptor, a nonraft marker, proteins separated using SDS-PAGE were electrophoretically transferred onto a polyvinylidene difluoride membrane (Millipore, Bedford, MA). Nonspecific binding was blocked with 5% fat-free milk in phosphate-buffered saline containing 0.1% Tween 20 (PBS-T). The blots were then incubated with a primary antibody overnight at 4°C. The monoclonal antibodies used were BA27, which is specific for the Aβ1–40 C-terminal site (Asami-Odaka et al., 1995), antiflotilin-1 antibody (BD Transduction Lab, San Jose, CA), and antitransferrin receptor antibody (Zymed, San Francisco, CA). The membrane was then incubated with a goat anti-mouse peroxidase-conjugated secondary antibody and visualized with SuperSignal chemiluminescence (Pierce, Rockford, IL) to obtain images on a film. For the detection of GM1 ganglioside, the membrane was probed with horseradish peroxidase-conjugated cholea toxin B (Sigma, St. Louis, MO; final concentration of 42 ng/ml) overnight at 4°C.

Isolation of Lipid Rafts From Rat Brain Cortex With or Without Synthetic Aβ1–40

An SD rat was anesthetized and its brain removed. One hundred milligrams of the isolated cerebral cortex were used for lipid raft isolation. The cerebral cortex in a glass/Teflon homogenizer tube (Iuchi, Osaka, Japan) was homogenized in 2.2 ml 1% Triton X-100/MBS [25 mM 2-(*N*-Morpholino) ethanesulfonic acid (MES) and 150 mM NaCl (pH 6.5) with 1% Triton X-100], including a mixture of protease inhibitors (Complete; Boehringer Mannheim, Mannheim, Germany), with or without 2.1 μM synthetic human Aβ1–40 (Peptide Institute Inc., Osaka, Japan). The brain fragments were homogenized with a glass/Teflon homogenizer (Iuchi) with 10 up-and-down strokes at 3,000 rpm on ice. The homogenates were then sonicated at 4°C and incubated for 1 hr on ice. The final Aβ1–40 concentration in the homogenate mixture was 2.1 μM. To prepare a stock solution of Aβ1–40, 0.5 mg Aβ1–40 was dissolved in 60 μl dimethylsulfoxide (DMSO), and the solution was then diluted with PBS to a final concentration of 200 μM. The lipid raft fraction was obtained from each homogenate as reported previously (Lisanti et al., 1994; Sawamura et al., 2001). One milliliter of each fraction was sequentially collected from the top of the gradient. The extraction of lipids and the subsequent determination of the concentration of cholesterol and phospholipids in each sample were carried out as reported previously (Michikawa et al., 2001).

Isolation of the Triton X-100-Insoluble Fraction From Tg2576 Mouse Brain

The Tg2576 mouse model of AD (Hsiao et al., 1996) at 13 months of age was anesthetized and the brain was removed. One hundred milligrams of the cerebral cortex in a glass/Teflon homogenizer tube (Iuchi) were homogenized in 2.2 ml 1% Triton X-100/MBS, pH 6.5, including a mixture of protease inhibitors (Complete; Boehringer Mannheim) with 10 up-and-down strokes at 3,000 rpm on ice. The homogenates were then sonicated at 4°C and incubated for 1 hr on ice. One hundred microliters of homogenate were then centrifuged at 100,000*g* for 1 hr at 4°C. The supernatant was removed and the resultant pellet was washed in MBS twice, resuspended in 50 μl of MBS, and subjected to highly sensitive immunoblot analysis with BA27 as a primary antibody.

Lipid Analysis

The concentrations of cholesterol and phospholipid in the samples were determined by using enzymatic methods as previously described (Gong et al., 2002). Cholesterol concentration was determined with a cholesterol determination kit, LTCII (Kyowa Medex, Tokyo, Japan), whereas phospholipid concentration was determined with a phospholipid determination kit, PLB (Wako, Osaka, Japan).

RESULTS AND DISCUSSION

Freshly dissolved Aβ1–40 remains as monomers, as demonstrated by immunoblot analysis and thioflavin-T assay as previously demonstrated (Zou et al., 2002). A rat brain was removed, and 100 mg of the cerebral cortex were isolated, to which 24 μl of 200 μM Aβ1– 40 were added. The cerebral cortex was then dissected into fragments in 2.2 ml of 1% Triton X-100/MBS containing protease inhibitors. The mixture was then homogenized with a glass/Teflon homogenizer (Iuchi) with 10 up-and-down strokes, followed by ultracentrifugation, as described in Materials and Methods. Samples from the 12 fractions were then obtained. The concentrations of cholesterol and phospholipids in each fraction were determined, and the recovery of GM1, a lipid raft marker, was demonstrated by electrophoresis, followed by labeling with horseradish peroxidase-conjugated choleatoxin. For the sample with Aβ1– 40, the main distributions peak of the cholesterol and phospholipids were found in the raft fractions, fractions 4–6, and most flotilin-1 and GM1, both of which are raft markers, was recovered in fractions 5 and 6 (Fig. 1a,c,e), whereas transferrin receptor, a nonraft maker, was recovered in fractions 10–12. This indicates that fractions 5 and 6 are the raft fractions. Similar results were obtained for the sample without exogenously added Aβ1– 40 (Fig. 1b,d,f).

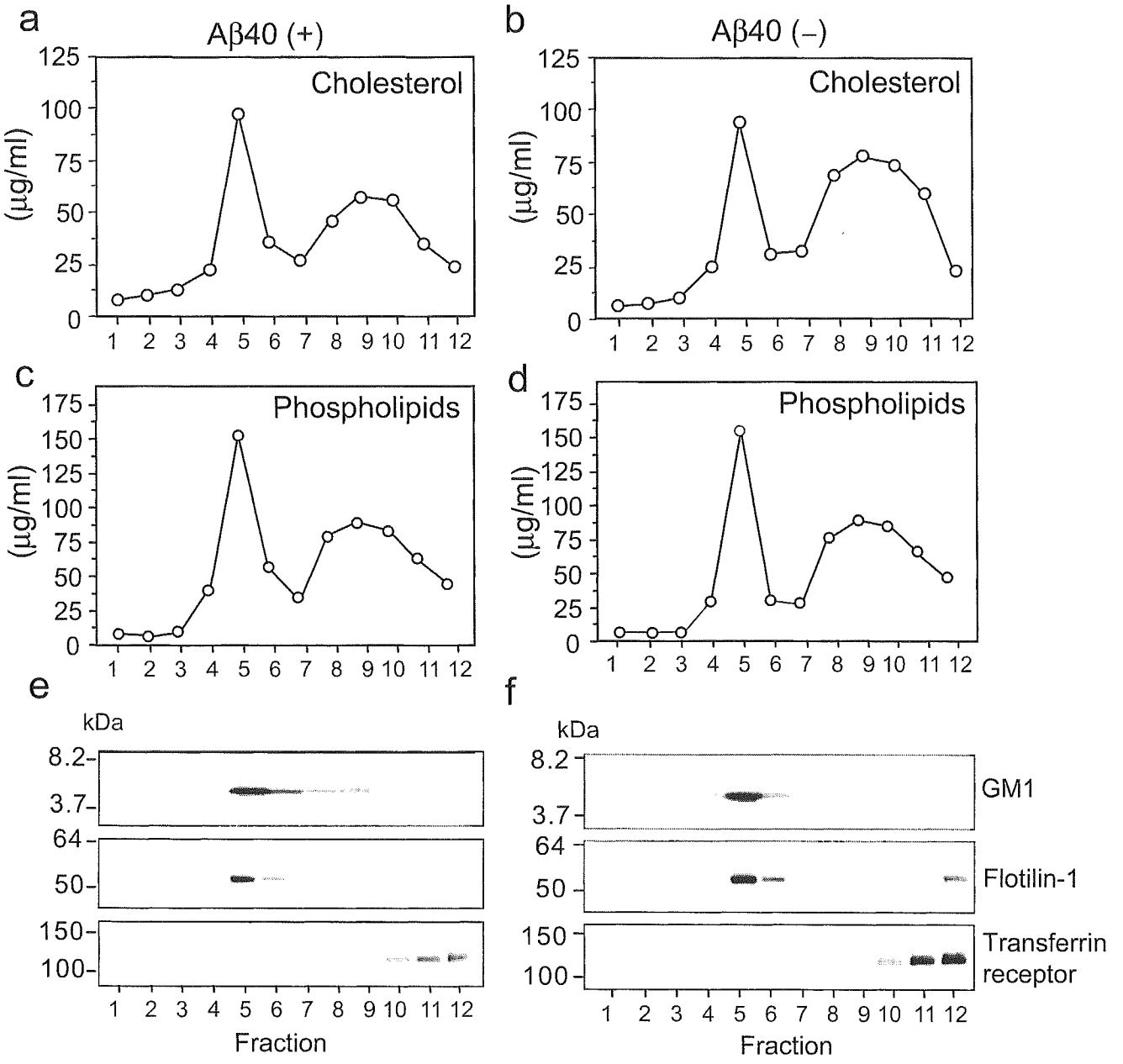

Fig. 1. Isolation of lipid raft fraction from a brain fragment with or without exogenous Aβ1–40. The brain fragment was subjected to homogenization in the presence of 1% Triton X-100/MBS with Aβ1–40 (2.1 μM; **a**,**c**,**e**) or without Aβ1–40 (**b**,**d**,**f**) and fractionated by sucrose density gradient centrifugation as described in Materials and Methods. The fractions were collected from the top gradient, and 11 fractions were obtained. The concentrations of cholesterol (**a**,**b**) and phospholipids (**c**,**d**) in each fraction were determined. The distribution of GM1 (**e**,**f**), a lipid raft marker, across the fractions was determined as described in Materials and Methods. Three independent experiments showed similar results.

We further analyzed the localization of Aβ1–40 in the above-mentioned fractions. Each sample was subjected to immunoblot analysis using the Aβ1–40-specific antibody BA27. Aβ1–40 accumulated and was highly oligomerized in fractions 4, 5, and 6 (Fig. 2a). No signal representing Aβ1–40 was detected in fraction 5, which was obtained by a method similar to that used for the sample without exogenously added Aβ1–40 (Fig. 2b). This indicates that signals representing the monomers and oligomers of Aβ1–40, as shown in Figure 2a, represent exogenously added Aβ1–40. We also analyzed a solution containing Aβ1–40 without a brain sample by sucrose-gradient ultracentrifugation, isolated fractions, and performed immunoblot analysis. Monomeric Aβ was detected in fractions 8–11, but no Aβ oligomers or Aβ accumulation were detected in the raft fraction (Fig. 2c). This is because the density of Aβ is higher

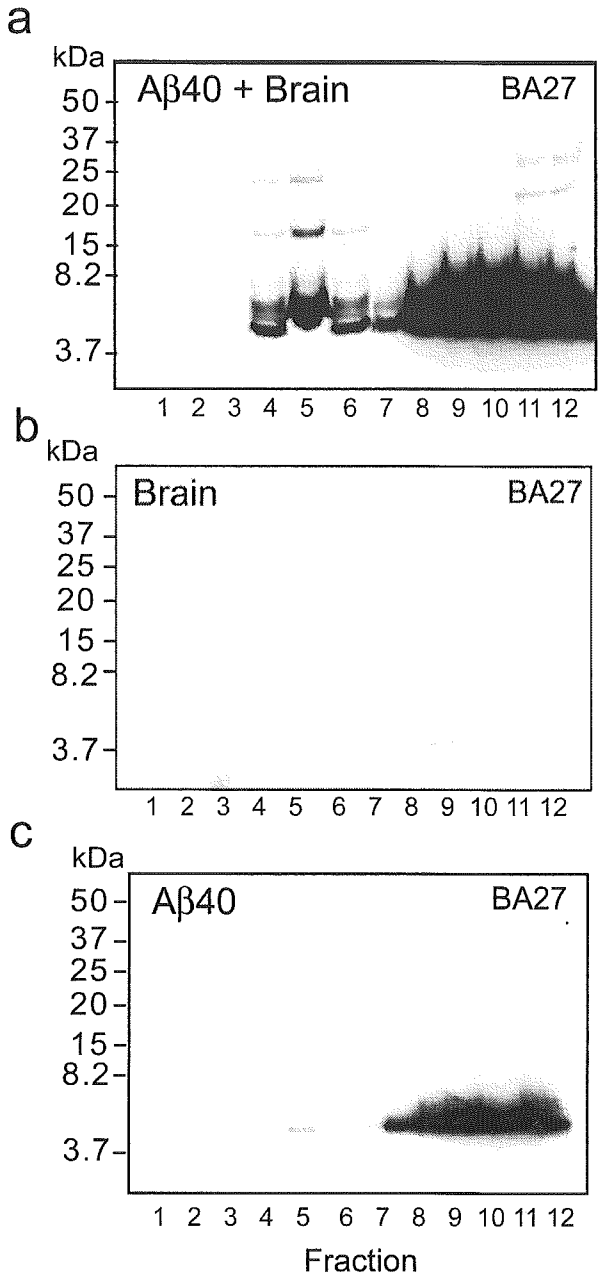

Fig. 2. Distribution of exogenously added Aβ1– 40 in lipid raft fractions. Brain fragments in the presence of 1% Triton X-100/MBS with (**a**) or without (**b**) exogenously added Aβ1– 40 (2.1 μM) were fractionated by sucrose density gradient centrifugation as described in Materials and Methods. Aβ1– 40 (2.1 μM) in 1% Triton X-100/MBS solution in the absence of brain fragments was also subjected to sucrose density gradient centrifugation (**c**). The fractions were collected from the top gradient, and 11 fractions were obtained. Immunoblot analysis using the anti-Aβ antibody BA27 was performed. Two independent experiments showed similar results.

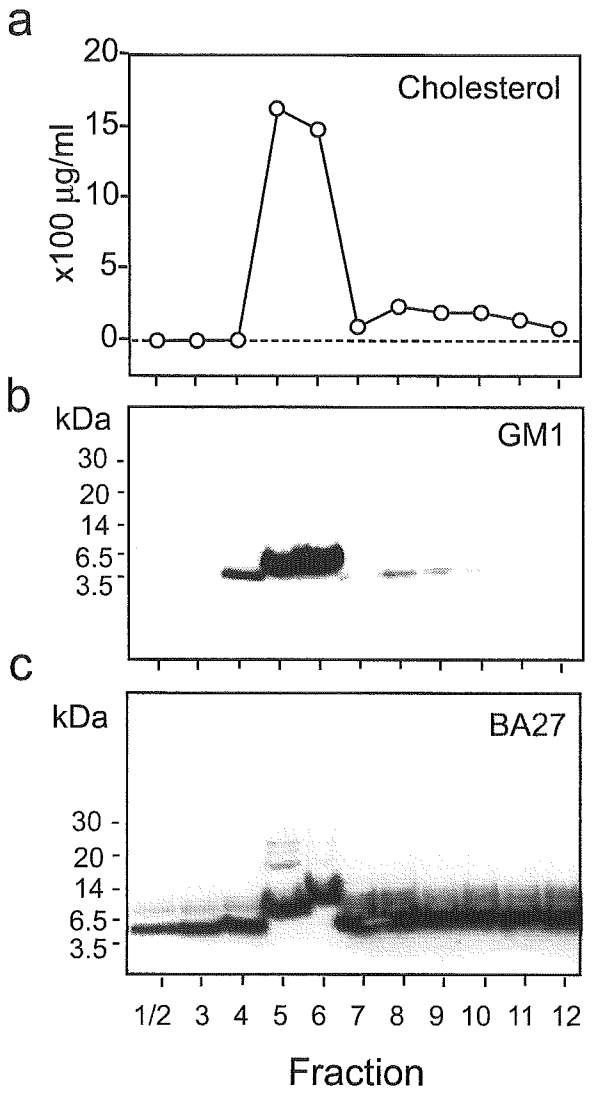

Fig. 3. Incubation of Aβ1– 40 in lipid rafts promoted Aβ1– 40 oligomerization. Brain homogenate in the presence of 1% Triton X-100/MBS without exogenously added Aβ1– 40 was fractionated by sucrose density gradient centrifugation as described in Materials and Methods. The distribution pattern of cholesterol (**a**) and GM1 (**b**) showed that fractions 5 and 6 are the lipid raft fractions. The aliquot of each fraction was incubated with 10 μM Aβ1– 40 for 20 hr at 4°C and subjected to immunoblot analysis using the anti-Aβ1–40 antibody BA27 (**c**).

than that of lipid rafts, so Aβ was recovered in fractions 8–11. The fact that exogenously added Aβ1–40 was recovered in the raft fraction indicates that Aβ1–40 binds to lipid rafts during the isolation of rafts, such as by homogenization, and that the binding of Aβ1–40 to lipid rafts leads to a shift in its localization to lower density fractions 4, 5, and 6.

Because the Aβ1–40 recovered in fraction 5 was highly oligomerized, we determined the effect of lipid rafts on Aβ oligomerization. We performed experiments to see the effect of incubating Aβ1–40 with raft and nonraft fractions on Aβ aggregation. The fractions were isolated from rat brain, and cholesterol concentration in each fraction was determined. The distribution patterns of cholesterol and GM1 across the fractions show that fractions 5 and 6 represent lipid raft fractions (Fig. 3a,b). The aliquot of each

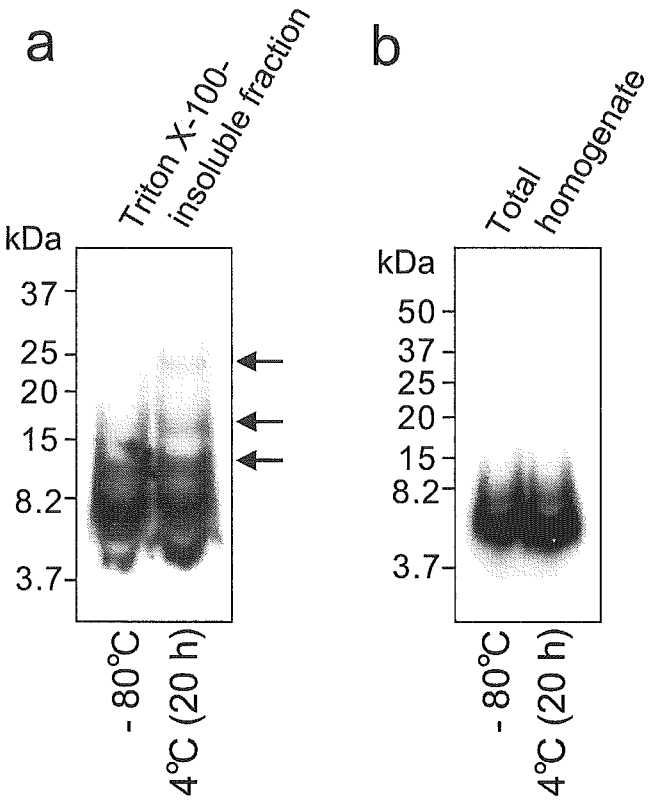

Fig. 4. Incubation of Triton X-100-insoluble fraction isolated from Tg2576 mouse brain promoted Aβ oligomerization. Brain homogenate from APP transgenic mouse (Tg2576) in the presence of 1% Triton X-100/MBS without exogenously added Aβ1– 40 was centrifuged, and the Triton X-100-insoluble fraction was obtained as described in Materials and Methods. Aliquots of total homogenate and the Triton X-100-insoluble fraction were immediately frozen at –80°C until use. Aliquots of each sample were also incubated for 20 hr at 4°C. The protein concentration of these samples was adjusted to 1.5 mg/ml. An equal amount of protein of each sample (20 μg protein/lane) was used for immunoblot analysis using BA27. Results of immunoblot analysis of the Triton X-100-insoluble fraction and total homogenate are shown in **a** and **b**, respectively.

fraction was incubated with 10 μM Aβ1–40 for 20 hr at 4°C and was subjected to immunoblot analysis using the anti-Aβ1–40 antibody BA27. Immunoblot analysis showed a marked oligomerization of Aβ1–40 in raft fractions 5 and 6 (Fig. 3c). This indicates that lipid rafts have an ability to promote Aβ1–40 oligomerization compared with other fractions. This notion is supported by a series of works showing that raft-like membranes rich in cholesterol and GM1 promote Aβ aggregation (Kakio et al., 2001, 2002).

The present results show that the isolation of lipid rafts promotes Aβ1–40 oligomerization when Aβ1–40 is added exogenously. The question arises, however, of whether this is also the case for endogenous Aβ, because the concentration of exogenous Aβ used in this study was much higher than that of endogenous Aβ in the brain. Therefore, we examined whether endogenous Aβ forms aggregates during the isolation of lipid rafts from the brains of Tg2576 mice, which overexpress human APP695 with "Swedish" mutation. The oligomerization of endogenous Aβ was not detected in lipid raft fractions, probably because of the low level of Aβ generated even in Tg2576 mouse brains (data not shown). Interestingly, however, the oligomerization of endogenous Aβ occurred in the Triton X-100-insoluble fraction, when the fraction was incubated at 4°C for 20 hr (Fig. 4a, right lane, arrows), which is the same duration for the isolation of rafts, whereas it did not in a nonincubated sample (Fig. 4a, left lane). The oligomerization of endogenous Aβ was not detected in samples of total homogenate even after the incubation (Fig. 4b). These results suggest that endogenous Aβ might have a potential for forming oligomers during the isolation of lipid rafts from brains. Overall, one should be careful in drawing conclusions regarding the association of Aβ with lipid rafts in terms of Aβ localization, oligomerization, or degradation, if one uses mainly a biochemical method. Even if one uses other assays, such as morphological analysis, it is still possible to overestimate the extent of Aβ metabolism occurring in lipid rafts.

ACKNOWLEDGMENT

We thank Takeda Chemical Industries Ltd. for providing antibody BA27.

REFERENCES

Alzneimer A. 1907. Uber eine eigenartige Erkrankung der Hirnrinde. Centralbl Nervenheilk Pscychiatr 30:177–179.

Asami-Odaka A, Ishibashi Y, Kikuchi T, Kitada C, Suzuki N. 1995. Long amyloid beta-protein secreted from wild-type human neuroblastoma IMR-32 cells. Biochemistry 34:10272–10278.

Bagnat M, Keranen S, Shevchenko A, Simons K. 2000. Lipid rafts function in biosynthetic delivery of proteins to the cell surface in yeast. Proc Natl Acad Sci U S A 97:3254–3259.

Ehehalt R, Keller P, Haass C, Thiele C, Simons K. 2003. Amyloidogenic processing of the Alzheimer beta-amyloid precursor protein depends on lipid rafts. J Cell Biol 160:113–123.

Esiri M, Hyman B, Beyreuther K, Masters C. 1997. Aging and dementia, vol 2. London: Arnold. p 153–233.

Estus S, Tucker HM, van Rooyen C, Wright S, Brigham EF, Wogulis M, Rydel R.E. 1997. Aggregated amyloid-beta protein induces cortical neuronal apoptosis and concomitant "apoptotic" pattern of gene induction. J Neurosci 17:7736–7745.

Fan QW, Yu W, Senda T, Yanagisawa K, Michikawa M. 2001. Cholesterol-dependent modulation of tau phosphorylation in cultured neurons. J Neurochem 76:391–400.

Geula C, Wu CK, Saroff D, Lorenzo A, Yuan M, Yankner BA. 1998. Aging renders the brain vulnerable to amyloid beta-protein neurotoxicity. Nat Med 4:827–831.

Gong JS, Kobayashi M, Hayashi H, Zou K, Sawamura N, Fujita SC, Yanagisawa K, Michikawa M. 2002. Apolipoprotein E (ApoE) isoform-dependent lipid release from astrocytes prepared from human ApoE3 and ApoE4 knock-in mice. J Biol Chem 277:29919–29926.

Gotz J, Chen F, van Dorpe J, Nitsch R.M. 2001. Formation of neurofibrillary tangles in P301l tau transgenic mice induced by Abeta 42 fibrils. Science 293:1491–1495.

Harder T, Simons K. 1997. Caveolae, DIGs, and the dynamics of sphingolipid-cholesterol microdomains. Curr Opin Cell Biol 9:534–542.

Hartley DM, Walsh DM, Ye CP, Diehl T, Vasquez S, Vassilev PM, Teplow DB, Selkoe DJ. 1999. Protofibrillar intermediates of amyloid beta-protein induce acute electrophysiological changes and progressive neurotoxicity in cortical neurons. J Neurosci 19:8876–8884.

Hsiao K, Chapman P, Nilsen S, Eckman C, Harigaya Y, Younkin S, Yang F, Cole G. 1996. Correlative memory deficits, Abeta elevation, and amyloid plaques in transgenic mice. Science 274:99–102.

Kakio A, Nishimoto SI, Yanagisawa K, Kozutsumi Y, Matsuzaki K. 2001. Cholesterol-dependent formation of GM1 ganglioside-bound amyloid beta-protein, an endogenous seed for Alzheimer amyloid. J Biol Chem 276:24985–24990.

Kakio A, Nishimoto S, Yanagisawa K, Kozutsumi Y, Matsuzaki K. 2002. Interactions of amyloid beta-protein with various gangliosides in raft-like membranes: importance of GM1 ganglioside-bound form as an endogenous seed for Alzheimer amyloid. Biochemistry 41:7385–7390.

Kawarabayashi T, Shoji M, Younkin LH, Wen-Lang L, Dickson DW, Murakami T, Matsubara E, Abe K, Ashe KH, Younkin SG. 2004. Dimeric amyloid beta protein rapidly accumulates in lipid rafts followed by apolipoprotein E and phosphorylated tau accumulation in the Tg2576 mouse model of Alzheimer's disease. J Neurosci 24:3801–3809.

Kojro E, Gimpl G, Lammich S, Marz W, Fahrenholz F. 2001. Low cholesterol stimulates the nonamyloidogenic pathway by its effect on the alpha-secretase ADAM 10. Proc Natl Acad Sci U S A 98:5815–5820.

Koudinov AR, Koudinova NV. 2001. Essential role for cholesterol in synaptic plasticity and neuronal degeneration. FASEB J 15:1858–1860.

Lambert MP, Barlow AK, Chromy BA, Edwards C, Freed R, Liosatos M, Morgan TE, Rozovsky I, Trommer B, Viola KL, Wals P, Zhang C, Finch CE, Krafft GA, Klein WL. 1998. Diffusible, nonfibrillar ligands derived from Abeta1–42 are potent central nervous system neurotoxins. Proc Natl Acad Sci U S A 95:6448–6453.

Lee SJ, Liyanage U, Bickel PE, Xia W, Lansbury PT Jr, Kosik KS. 1998. A detergent-insoluble membrane compartment contains A beta in vivo. Nat Med 4:730–734.

Lisanti MP, Scherer PE, Vidugiriene J, Tang Z, Hermanowski-Vosatka A, Tu YH, Cook RF, Sargiacomo M. 1994. Characterization of caveolin-rich membrane domains isolated from an endothelial-rich source: implications for human disease. J Cell Biol 126:111–126.

Lorenzo A, Yankner BA. 1994. Beta-amyloid neurotoxicity requires fibril formation and is inhibited by Congo red. Proc Natl Acad Sci U S A 91:12243–12247.

Mattson MP, Tomaselli KJ, Rydel RE. 1993. Calcium-destabilizing and neurodegenerative effects of aggregated β-amyloid peptide are attenuated by basic FGF. Brain Res 621:35–49.

Michikawa M, Gong JS, Fan QW, Sawamura N, Yanagisawa K. 2001. A novel action of Alzheimer's amyloid β-protein (Aβ): oligomeric Aβ promotes lipid release. J Neurosci 21:7226–7235.

Morishima Y, Gotoh Y, Zieg J, Barrett T, Takano H, Flavell R, Davis RJ, Shirasaki Y, Greenberg ME. 2001. Beta-amyloid induces neuronal apoptosis via a mechanism that involves the c-Jun N-terminal kinase pathway and the induction of Fas ligand. J Neurosci 21:7551–7560.

Morishima-Kawashima M, Ihara Y. 1998. The presence of amyloid beta-protein in the detergent-insoluble membrane compartment of human neuroblastoma cells. Biochemistry 37:15247–15253.

Oshima N, Morishima-Kawashima M, Yamaguchi H, Yoshimura M, Sugihara S, Khan K, Games D, Schenk D, Ihara Y. 2001. Accumulation of amyloid beta-protein in the low-density membrane domain accurately reflects the extent of beta-amyloid deposition in the brain. Am J Pathol 158:2209–2218.

Pike CJ, Burdick D, Walencewicz AJ, Glabe CG, Cotman CW. 1993. Neurodegeneration induced by β-amyloid peptides in vitro: the role of peptide assembly state. J Neurosci 13:1676–1687.

Sargiacomo M, Sudol M, Tang Z, Lisanti MP. 1993. Signal transducing molecules and glycosyl-phosphatidylinositol-linked proteins form a caveolin-rich insoluble complex in MDCK cells. J Cell Biol 122:789–807.

Sawamura N, Gong JS, Garver WS, Heidenreich RA, Ninomiya H, Ohno K, Yanagisawa K, Michikawa M. 2001. Site-specific phosphorylation of tau accompanied by activation of mitogen-activated protein kinase (MAPK) in brains of Niemann-Pick type C mice. J Biol Chem 276:10314–10319.

Sawamura N, Ko M, Yu W, Zou K, Hanada K, Suzuki T, Gong JS, Yanagisawa K, Michikawa M. 2004. Modulation of amyloid precursor protein cleavage by cellular sphingolipids. J Biol Chem 279:11984–11991.

Selkoe DJ. 1994. Alzheimer's disease: a central role for amyloid. J Neuropathol Exp Neurol 53:438–447.

Simons K, Ikonen E. 1997. Functional rafts in cell membranes. Nature 387:569–572.

Simons M, Keller P, De Strooper B, Beyreuther K, Dotti CG, Simons K. 1998. Cholesterol depletion inhibits the generation of β-amyloid in hippocampal neurons. Proc Natl Acad Sci U S A 95:6460–6464.

Sponne I, Fifre A, Drouet B, Klein C, Koziel V, Pincon-Raymond M, Olivier JL, Chambaz J, Pillot T. 2003. Apoptotic neuronal cell death induced by the nonfibrillar amyloid-beta peptide proceeds through an early reactive oxygen species-dependent cytoskeleton perturbation. J Biol Chem 278:3437–3445.

Sudoh S, Kawamura Y, Sato S, Wang R, Saido TC, Oyama F, Sakaki Y, Komano H, Yanagisawa K. 1998. Presenilin 1 mutations linked to familial Alzheimer's disease increase the intracellular levels of amyloid beta-protein 1-42 and its N-terminally truncated variant(s) which are generated at distinct sites. J Neurochem 71:1535–1543.

Walsh DM, Klyubin I, Fadeeva JV, Cullen WK, Anwyl R, Wolfe MS, Rowan MJ, Selkoe DJ. 2002. Naturally secreted oligomers of amyloid beta protein potently inhibit hippocampal long-term potentiation in vivo. Nature 416:535–539.

Zou K, Gong JS, Yanagisawa K, Michikawa M. 2002. A novel function of monomeric amyloid beta-protein serving as an antioxidant molecule against metal-induced oxidative damage. J Neurosci 22:4833–4841.

THE JOURNAL OF BIOLOGICAL CHEMISTRY
Vol. 280, No. 12, Issue of March 25, pp. 11731–11739, 2005
Printed in U.S.A.

Altered Cholesterol Metabolism in Niemann-Pick Type C1 Mouse Brains Affects Mitochondrial Function*[S]

Received for publication, November 15, 2004, and in revised form, January 10, 2005
Published, JBC Papers in Press, January 11, 2005, DOI 10.1074/jbc.M412898200

Wenxin Yu‡, Jian-Sheng Gong‡§, Mihee Ko‡, William S. Garver¶, Katsuhiko Yanagisawa‡, and Makoto Michikawa‡‖

From the ‡Department of Alzheimer's Disease Research, National Institute for Longevity Sciences, 36-3 Gengo, Morioka, Obu, Aichi 474-8522, Japan, §The Pharmaceuticals and Medical Devices Agency, Tokyo 100-0013, Japan, and the ¶Department of Pediatrics, The University of Arizona, Tucson, Arizona 85724

Niemann-Pick type C1 (NPC1) disease is a fatal hereditary disorder characterized by a defect in cholesterol trafficking and progressive neurodegeneration. Although the NPC1 gene has been identified, the molecular mechanism responsible for neuronal dysfunction in brains of patients with NPC1 disease remains unknown. This study demonstrates that the amount of cholesterol within mitochondria membranes is significantly elevated in NPC1 mouse brains and neural cells. In addition, the mitochondrial membrane potential, the activity of ATP synthase, and henceforth the level of ATP are markedly decreased in NPC1 mouse brains and neurons. Importantly, reducing the level of cholesterol within mitochondrial membranes using methyl-β-cyclodextrin can restore the activity of ATP synthase. Finally, NPC1 neurons show an impaired neurite outgrowth, which can be rescued by exogenous ATP. These results suggest that mitochondrial dysfunctions and subsequent ATP deficiency, which are induced by altered cholesterol metabolism in mitochondria, may be responsible for neuronal impairment in NPC1 disease.

Niemann-Pick type C1 (NPC1)[1] disease is an autosomal recessive disorder characterized by progressive neurodegeneration including ataxia, dystonia, seizures, and dementia (1). Biochemical and cellular analysis has shown that low density lipoprotein-derived cholesterol accumulates in late endosome/lysosomes, with delayed cholesterol transport to cellular compartments responsible for the regulation of intracellular cholesterol homeostasis (2–4). In addition to cholesterol, glycosphingolipids and other lipids accumulate in NPC1 brains (1, 5), which possibly induce symptoms associated with NPC1 disease (6).

The gene responsible for NPC1 disease, *NPC1*, was identified in both humans and mice, and subsequently cloned (7, 8). Studies have demonstrated that NPC1 is associated with a novel late endosomal/lysosomal compartment that facilitates the transport of cholesterol to the trans-Golgi network, plasma membrane, and endoplasmic reticulum (9–12). The neuropathology associated with NPC1 dysfunction is characterized by distended neurons, an accumulation of lipid storage bodies, presence of dendritic and axonal abnormalities, and eventually neuronal loss (13–15). However, it remains undefined whether it is the accumulation of cholesterol and/or gangliosides responsible for the disease phenotype. In this context, it has proven beneficial to utilize the BALB/c NPC1 mouse with homozygous NPC1 mutations that displays a biochemical phenotype similar to patients with NPC1 disease, including neurodegeneration (16), irregular dendritic trees and spines (17), and progressive tauopathy (5, 18). There have been a number of different hypotheses formulated to explain the molecular basis of neurodegeneration in NPC1 disease. The continuous defective use of cholesterol in NPC1 neural tissues has been suggested to cause tauopathy (5, 18, 19). With respect to neuronal gangliosides, although some studies support the case for an accumulation of gangliosides causing neurodegeneration (20), another study indicates that an accumulation of gangliosides is not the cause for neurodegeneration in NPC1 mice (21). A more recent study has demonstrated that impaired neurosteroidogenesis, because of disordered cholesterol trafficking, affects neuronal growth and differentiation, and that allopregnanolone treatment delays the onset of neurological symptoms and lengthens the lifespan of NPC1 mice (22). However, the mechanism causing disrupted neurosteroidogenesis in NPC mice remains unclear.

In this report, the BALB/c NPC1 mouse model was used to investigate the molecular basis for neuronal impairment in NPC1 disease. The results reveal a novel mechanism whereby an increased level of cholesterol in mitochondria membranes adversely affects the mitochondrial membrane potential, synthesis of ATP, and the level of cellular ATP in NPC1 mouse brains and neurons. Importantly, neuronal impairment in neurite outgrowth was restored by the addition of ATP, providing a potentially useful therapy for NPC1 disease.

EXPERIMENTAL PROCEDURES

BALB/c NPC1^{NIH} Mice—The animal care and experiments using animals were carried out in accordance with the institutional guidelines. A breeding pair of BALB/c NPC1^{NIH} mice, heterozygous for NPC1 (NPC1+/−), were obtained from Jackson Laboratory (Bar Harbor, MA). These heterozygous mice were maintained on a low-cholesterol diet (w/w) and low fat 6% (w/w) normal mouse diet. These mice were bred to produce normal (NPC1+/+), heterozygous (NPC1+/−), and homozygous affected (NPC1−/−) mice. For all experiments using brain samples from cerebral cortices in this report, only male mice at 9 weeks of

* This work was supported by Longevity Sciences Grant H14-10 from the Ministry of Health, Labor and Welfare, a grant from the Pharmaceuticals and Medical Devices Agency, Japan, and in part by the National Niemann-Pick Disease Foundation, Inc., USA. The costs of publication of this article were defrayed in part by the payment of page charges. This article must therefore be hereby marked "*advertisement*" in accordance with 18 U.S.C. Section 1734 solely to indicate this fact.

[S] The on-line version of this article (available at http://www.jbc.org) contains Figs. S1 and S2.

‖ To whom correspondence should be addressed: Dept. of Alzheimer's Disease Research, National Institute for Longevity Sciences, 36-3 Gengo, Morioka, Obu, Aichi 474-8522, Japan. Tel.: 81-562-46-2311; Fax: 81-562-46-3157; E-mail: michi@nils.go.jp.

[1] The abbreviations used are: NPC1, Niemann-Pick type C1; VDAC, voltage-dependent anion channel; PBS, phosphate-buffered saline; DMEM, Dulbecco's modified Eagle's medium; IM, inner membrane; OM, outer membrane; CS, contact site; PC, phosphatidylcholine; HDL, high density lipoprotein; UCP, uncoupling protein; AMP-PNP, 5′-adenylyl-β,γ-imidodiphosphate; AD, Alzheimers disease.

age were investigated. For preparation of primary cultures, the cerebral cortices from embryonic day 16 or postnatal day 2 mouse brains were used.

Genotype Analysis—For genotype analysis of mice and cultured cells prepared from embryos or postnatal day 2 mice, DNA was isolated from the tail tips of each mouse and PCR was performed at the *NPC1* locus using primer pairs as previously described (7).

Antibodies—Mouse monoclonal antibodies against cytochrome *c* (a mitochondrion marker), Na^+,K^+-ATPase $\beta 2$ (a plasma membrane marker), GM130 (a Golgi marker), nucleoporin p62 (a nucleus marker), and Bip/GRP78 (an endoplasmic reticulum marker) were purchased from BD Pharmingen. Mouse monoclonal antibodies against cathepsin L (a lysosome marker) and cytochrome oxidase subunit I (a mitochondrial inner membrane marker) were purchased from Transduction Laboratory (Lexington, KY) and Molecular Probes, Inc. (Eugene, OR), respectively. Rabbit polyclonal antibodies against voltage-dependent anion channel (VDAC: a mitochondrial outer membrane marker), fumarase (a mitochondrial matrix maker), and UCP2 (the uncoupling protein) were purchased from Affinity Bioreagents (Golden, CO), Nordic Immunological Laboratory (Tilburg, the Netherlands), and Santa Cruz Biotechnology, Inc. (Santa Cruz, CA), respectively.

Electron Microscopy—Electron microscopy was performed as previously described (5). In brief, the cerebella removed from NPC1+/+ and NPC1−/− mice at 9 weeks old were rinsed with PBS and fixed and embedded in epoxy resin. Ultrathin sections were double-stained with 2.0% uranyl acetate for 10 min and with a lead-staining solution for 5 min, and then examined using a JEOL JEM-1200EX transmission electron microscope.

Cell Culture—The embryonic brains were removed on embryonic day 16 for neuronal cultures. The genotype of each embryo was determined using the tail as described above. Neuron-rich cultures were prepared from the cerebral cortex as previously described (23). Dissociated cells were suspended in medium consisting of Dulbecco's modified Eagle's medium nutrient mixture (DMEM/F-12; 50%: 50%), N2 supplements, and 0.1% bovine serum albumin (BSA) and plated onto poly-D-lysine-coated 6-well plates at a cell density of $2 \times 10^4/cm^2$. On day 3 of culture, more than 99% of the cultured cells were identified as neurons by immunocytochemical analysis using a monoclonal antibody against microtubule-associated protein 2 (Sigma), a neuron-specific marker. To prepare astrocyte-rich cultures, the brains from postnatal day 2 mice were removed under anesthesia. After genotype analysis, the cortex was dissociated and cortical cells were seeded in 75-cm^2 dishes at a cell density of 1×10^7 in DMEM containing 10% fetal bovine serum as previously described (24). After 10 days of incubation *in vitro*, astrocytes in the monolayer were trypsinized (0.1%) and reseeded into 6-well plates. The astrocyte-rich cultures were maintained in DMEM containing 10% fetal bovine serum until use.

Mitotracker Labeling—Primary neurons and astrocytes cultured for 5 and 14 days, respectively, were rinsed three times with PBS and then incubated in Hanks' balanced salt solution containing 3 μM Mitotracker JC-1 (Molecular Probes, Inc.) for 20 min at 37 °C. Stock solutions of 600 μM Mitotracker JC-1 were prepared in dimethyl sulfoxide (Me_2SO). Mitotracker JC-1 was rinsed from cells using Hanks' balanced salt solution and then cells were allowed to equilibrate in Hanks' balanced salt solution at room temperature for an additional 20 min. Fluorescent images were obtained using a model LSM 510 laser scanning confocal microscope (Carl Zeiss Co., Ltd., Jena, Germany) equipped with a ×63 Plan Apochromat numerical aperture and 1.4 oil immersion objective. Simultaneous two-channel recording was performed using excitation wavelength lines of 488 and 543 nm of an argon laser, and fluorescence was detected using 530 and 590 nm emission filters. For merged images, images were adjusted to similar intensities and then merged using Adobe Photoshop 6.0.

Determination of ATP Levels in Tissues and Cultured Cells—The brain, liver, and muscle were removed and homogenates were prepared with PBS containing protease inhibitors, Complete™ (Roche Diagnostics), using a glass/Teflon homogenizer (Iuchi, Osaka, Japan) with 10 up and down strokes at 1,000, 2,000, and 3,000 rpm, respectively. The homogenates were centrifuged at 10,000 × *g* for 2 min at 4 °C, and then rinsed three times with PBS. For preparation of homogenates of cultured cells, harvested cultured cells in PBS containing protease inhibitors, Complete™, were homogenized using a glass/Teflon homogenizer, followed by centrifugation at 10,000 × *g* for 2 min at 4 °C, and then rinsed three times with PBS. The level of ATP in these samples was determined using the ATP Bioluminescence Assay Kit CLS II (Roche). In brief, this was performed by resuspending the pellet into 50 μl of ice-cold ATP-lysis buffer (100 mM Tris and 4 mM EDTA, pH 7.75), to which 150 μl of boiling ATP-lysis buffer was added, and the samples were incubated for 2 min at 99 °C. The samples were centrifuged at 10,000 × *g* for 1 min at 4 °C, and the resulting supernatants collected. Finally, the level of ATP was determined by combining 50 μl of the supernatant with 50 μl of luciferase reagent. After a 1.6-s delay, chemiluminescence was measured with a 10-s integration time using a microplate luminometer (EG&G Berthold, Bad Wildbad, Germany). Luciferase activity was expressed as fluorescence units per μg of protein.

Isolation of Brain Mitochondria—Cerebral cortices were isolated and homogenized in the isolation buffer (5 mM HEPES, pH 7.4, 250 mM mannitol, 1 mM EGTA, 70 mM sucrose, and 0.1% fat-free BSA) using a glass/Teflon homogenizer (Iuchi, Osaka, Japan) with 10 up and down strokes. The homogenates were centrifuged at 600 × *g* for 10 min at 4 °C, with the resulting pellet being suspended into isolation buffer (P1), and the resulting supernatant (S1) being centrifuged at 10,300 × *g* for 15 min at 4 °C in a Beckman SW 41 rotor. The resulting supernatant (S2), was stored and the pellet (P2) was suspended in 2 ml of isolation buffer, loaded onto 8 ml of 30% (v/v) Percoll in gradient buffer (25 mM HEPES, pH 7.4, 225 mM mannitol, 1 mM EGTA, and 0.1% fat-free BSA), and centrifuged at 95,000 × *g* for 30 min at 4 °C. The resulting supernatant (S3) was stored, and the mitochondrial pellet (P3) was rinsed with isolation buffer by centrifuging 15 min at 7,000 × *g* at 4 °C, and then resuspended in isolation buffer. Protein concentration was determined by the bicinchoninic protein determination method (Pierce Chemical Co.).

Subfractionation of Brain Mitochondria by Digitonin—A 2.0% digitonin stock solution was prepared immediately prior to use by dissolving digitonin in the isolation solution (210 mM mannitol, 1 mM EGTA, 70 mM sucrose) as previously described (25). One ml of ice-cold digitonin solution was added to 1 ml of mitochondrial protein (100 mg/ml). The resulting suspension was homogenized, and then centrifuged at 12,000 × *g* for 5 min at 4 °C. The supernatant was removed, and the pellet was resuspended in the same volume of isolation solution. This suspension was centrifuged again at 12,000 × *g* for 10 min. The pellet from the second centrifugation is hereafter referred to as the "inner membrane" (IM). The supernatants from the first and second centrifugation were pooled, and fractionated by centrifugation at 144,000 × *g* for 1 h at 4 °C. The pellet from this centrifugation is hereafter referred to as the "outer membrane" (OM) and the supernatant the "contact sites" (CS) (26).

Enzymatic Analysis of Complex I + III, II + III, IV, and V—The mitochondria isolated from homogenates of cerebral cortices were used for enzymatic analysis. (*a*) The enzyme activity of NADH-cytochrome *c* oxidoreductase (complex I + III) was determined as previously described (27). In brief, a 150-μl reaction buffer (50 mM K_2HPO_4, pH 7.4, 0.1 mM NADH, 0.1 mM cytochrome *c*, and 0.3 mM KCN) with and without 1.5 μM rotenone, was incubated for 5 min at 30 °C, followed by the addition of 10 μl of mitochondria protein (3 μg/μl). NADH-cytochrome *c* oxidoreductase activity was immediately monitored at 550 nm and the difference in the reduction of cytochrome *c* with and without rotenone was calculated. (*b*) The enzyme activity of succinate-cytochrome *c* oxidoreductase (complex II + III) was determined as previously described (28). In brief, a 150-μl reaction buffer (40 mM K_2HPO_4, pH 7.4, 20 mM sodium succinate, 50 μM cytochrome *c*, 0.5 mM EDTA, and 0.25 mM KCN) was incubated for 5 min at 30 °C, followed by the addition of 10 μl of mitochondrial protein (3 μg/μl). Succinate-cytochrome *c* oxidoreductase activity was monitored at 550 nm and the difference in the reduction of cytochrome *c* was calculated. (*c*) The enzyme activity of cytochrome *c* oxidase (complex IV) was determined as previously described (29). Complex IV activity was measured as the oxidation of ferrocytochrome *c* by cytochrome *c* oxidase at 550 nm. Ferrocytochrome *c* was first prepared from 10% cytochrome *c* by reduction with sodium ascorbate and dialysis against 0.01 M K_2HPO_4 (pH 7.0) using a 3.5-kDa exclusion dialysis membrane. A 150-μl reaction buffer (10 mM K_2HPO_4, pH 7.4, 70 μl of ferrocytochrome *c*) was incubated 5 min at 30 °C, followed by the addition of 10 μl of mitochondrial protein (3 μg/μl). Cytochrome *c* oxidase activity was immediately monitored at 550 nm. (*d*) The enzyme activity of mitochondrial complex V was determined as previously described (29). ATPase activity was measured as the hydrolysis rate of ATP determined by a bioluminescence method. In brief, a 250-μl reaction buffer (10 mM K_2HPO_4, pH 7.4, 300 mM D-mannitol, 10 mM KCl, 5 mM $MgCl_2$, 1 mg/ml BSA, 2 μM rotenone, 0.3 mM KCN) was combined with 100 μg of mitochondrial protein. The reaction was initiated by adding 1.5 μl of 500 mM ATP (at a final concentration of 3 mM) and run for 15 min at 37 °C then stopped by adding oligomycin at a final concentration of 10 μM. A control experiment was performed under the same conditions in the presence of 10 μM oligomycin to obtain the nonenzymatic hydrolysis of ATP. The solution was diluted to 1/10 and the ATP level was measured by the luciferin-

luciferase method using the ATP Bioluminescence Assay Kit CLS II (Roche) in a luminescence spectrometer.

For the determination of ATP synthase activity, 100 μg of mitochondrial protein from each sample was used to measure the synthesis of ATP. The reaction was initiated by adding 100 μg of mitochondrial protein into 100 μl of reaction buffer (10 mM K_2HPO_4, pH 7.4, 300 mM D-mannitol, 10 mM KCl, and 5 mM $MgCl_2$) at 37 °C. After a period of 1 min, 10 μl of ADP (50 μM) was added, and the intensity of bioluminescene was recorded at 37 °C, where the peak height was proportional to the amount of ATP that was synthesized.

Effect of Removal of Cholesterol from the Mitochondria Membrane—To remove cholesterol from the mitochondria membrane, a stock solution of methyl-β-cyclodextrin (Sigma) (150 mM) was prepared using distilled water, and then diluted into the P2 fraction derived from brains to a final concentration of 7.5 mM. The mixture was incubated for 20 min at 37 °C, followed by an additional incubation for 10 min at room temperature and subjected to ultracentrifugation to purify mitochondria. For the cholesterol enrichment of mitochondria with or without methyl-β-cyclodextrin, a stock solution of cholesterol was prepared (5 mM in 100% ethanol) and added into the P2 fraction that was resuspended in isolation buffer (200 μl) at a final concentration of 50 μM, followed by incubation for 20 min at 37 °C. The mitochondria were rinsed twice and subjected to ultracentrifugation to purify mitochondria. The cholesterol level, protein content, and the ATP synthase activity associated with mitochondria were then determined as described above.

Immunoblot Analysis—Immunoblot analysis was performed as previously described (5). The primary antibodies used were mouse monoclonal antibodies (cytochrome *c*, 1:1,000 dilution; Na^+,K^+-ATPase β2, 1:1000 dilution; GM130, 1:500 dilution; Bip/GRP78, 1:500 dilution; cathepsin L, 1:1000 dilution; nucleoporin p62, 1:1000 dilution; and cytochrome *c* oxidase subunit I, 1:1000 dilution), and rabbit polyclonal antibodies (VDAC, 1:1000 dilution; fumarase, 1:500 dilution; and UCP-2, 1:1,000 dilution). After rinsing and incubation in the presence of appropriate peroxidase-conjugated secondary antibody, the respective bands were detected with an ECL kit (Amersham Biosciences).

Morphological Analysis—Cultured neurons maintained for 1, 2, and 3 days in serum-free medium in the presence or absence of 0.5 mM ATP, 0.5 mM ADP, or 0.5 mM AMP-PNP (Roche) were rinsed and then fixed for 20 min at room temperature in 0.1 M PBS containing 4% paraformaldehyde fluoride. The cells were then rinsed with PBS, blocked in PBS containing 2.0% BSA, then incubated with monoclonal anti-β-tubulin antibody (Covance, Richmond, CA, 1:500 dilution) in PBS containing 2% BSA overnight at 4 °C. The cells were then incubated with anti-mouse IgG (1:200) in 0.1 M PBS, 0.5% BSA for 1 h, rinsed, and visualized using the ABC method. Photographic images were captured using a CCD camera (DC500) (Leica Microsystems GMBH, Wetzar, Germany) attached with phase-contrast microscopy (Olympus IX70, Olympus Co. Ltd., Tokyo, Japan). The ratio of neurite number/cell and neurite total length/cell was determined using an image analyzer (LSM 510, Carl Zeiss Co., Ltd., Jena, Germany).

Determination of Cholesterol and Phosphatidylcholine (PC) Transport—To determine the transport of exogenously added cholesterol and PC into mitochondria in cultured cells, wild type astrocytes were labeled with 37 Bq/ml of [^{14}C]acetate (PerkinElmer Life Sciences). The conditioned media was collected 5 days later and an equivalent amount of ^{14}C-labeled HDL (cholesterol concentration at 1 μg/ml) was added into plates previously seeded with NPC1+/+, NPC1+/−, and NPC1−/− astrocytes. The cells were harvested at 4, 8, and 12 h following the addition of HDL and the mitochondria were isolated. The lipids were separated using sequential one-dimensional chromatography and the amounts of [^{14}C]cholesterol and [^{14}C]PC were quantified using BAS2500 (Fuji Film, Tokyo, Japan) as previously described (24).

To measure lipid efflux from mitochondria and cells, cultured astrocytes were labeled for 5 days with ^{14}C-labeled HDL. Five days following the commencement of labeling, the cells were rinsed in DMEM three times and incubated in DMEM. The cells were then harvested at 0, 2, and 4 h, and mitochondria were isolated from each culture. The amounts of [^{14}C]cholesterol and [^{14}C]PC remaining in the mitochondria and cells were determined as described above.

Lipid Analysis—The concentration of cholesterol was determined using a cholesterol determination kit, LTCII (Kyowa Medex, Tokyo), whereas the concentration of phospholipids was determined using a phospholipid determination kit, PLB (Wako, Osaka, Japan), as previously described (24).

Statistical Analysis—Statistical analysis was performed using StatView computer software, and multiple pairwise comparisons among groups of data were performed using the analysis of variance, and the Bonferroni *t* test.

RESULTS

The Morphology and Membrane Potential of Mitochondria in Neurons and Astrocytes Isolated from Mouse Brains—The morphology and function of mitochondria were examined in NPC1+/+, NPC1+/−, and NPC1−/− mouse brains, and cultured cells prepared from cerebral cortices using electron and confocal microscopy. The examination of NPC1+/+ and NPC1−/− mouse brains using electron microscopy revealed that NPC1−/− mouse brains contained smaller and more rounded mitochondria, with a translucent matrix and irregular cisternae (Fig. 1, *a* and *b*). Next, the membrane potential of mitochondrial membrane within cultured neurons and astrocytes was determined using Mitotracker JC-1 (30). When mitochondrial membrane potential is normally polarized, JC-1 concentrates in the mitochondria and aggregates, resulting in a high red/green fluorescence intensity ratio. However, with decreasing mitochondrial membrane potential, there is less aggregation of Mitotracker JC-1, therefore resulting in decreased red/green fluorescence intensity ratio. The results indicated a marked decrease in red fluorescence intensity in NPC1−/− neurons (Fig. 1*e*) compared with NPC1+/+ (Fig. 1*c*) and NPC1+/− neurons (Fig. 1*d*). In contrast, there was a marked increase in green fluorescence intensity observed in NPC1−/− neurons (Fig. 1*h*), compared with NPC1+/+ neurons (Fig. 1*f*) and NPC1+/− neurons (Fig. 1*g*). Similarly, there was a marked decrease in red fluorescence intensity in NPC1−/− astrocytes (Fig. 1*n*) compared with NPC1+/+ neurons (Fig. 1*l*) and NPC1+/− astrocytes (Fig. 1*m*) and a marked increase in green fluorescence intensity in NPC1−/− astrocytes (Fig. 1*q*) compared with NPC1+/+ astrocytes (Fig. 1*o*) and NPC1+/− astrocytes (Fig. 1*p*). However, this being the case, there was no significant difference noticed in the survival of NPC1+/+, NPC1+/−, and NPC1−/− neurons and astrocytes (data not shown). Together, these results indicate that NPC1−/− neurons and astrocytes have an altered structure and altered membrane potential of mitochondria.

The Level of ATP in Brain, Muscle, Liver, and Cultured Cortical Neurons—The level of ATP was determined in brain, muscle, and liver from NPC1+/+, NPC1+/−, and NPC1−/− mice at 9 weeks of age. The results indicate that the level of ATP in these tissues derived from NPC1−/− mice are significantly decreased compared with that derived from NPC1+/+ and NPC1+/− mice (Fig. 2*a*). As an internal control for the amount of mitochondria used in each sample, immunoblot analysis was performed to determine the amount of VDAC, a protein that resides in the outer membrane of mitochondria (Fig. 2, *insets*). The addition of ATP into the liver samples (20 nmol of ATP/mg of protein) resulted in increased levels of ATP by ~15 nmol/mg of protein in the three genotypes, excluding a possibility that the ATP degradation rate is accelerated in NPC1−/− tissues. The level of ATP was also determined in cultured cortical neurons prepared from NPC1+/+, NPC1+/−, and NPC1−/− mice at embryonic day 16, and maintained and harvested at days 3 and 6 of culture (Fig. 2*b*). The results again indicate that the level of ATP in neurons prepared from NPC1−/− mouse brains are significantly decreased compared with neurons prepared from NPC1+/+ and NPC1+/− mouse brains.

Enzymatic Analysis of Mitochondria Complexes I + III, II + III, IV, and V Using Purified Mitochondria from Mouse Brains—To determine which step(s) in ATP metabolism might be affected in NPC1−/− cells, the activities of respiratory complex I + III (NADH-cytochrome *c* oxidoreductase), complex II + III (succinate-cytochrome *c* oxidoreductase), complex IV (cytochrome *c* oxidase), and ATP synthase (complex V) were deter-

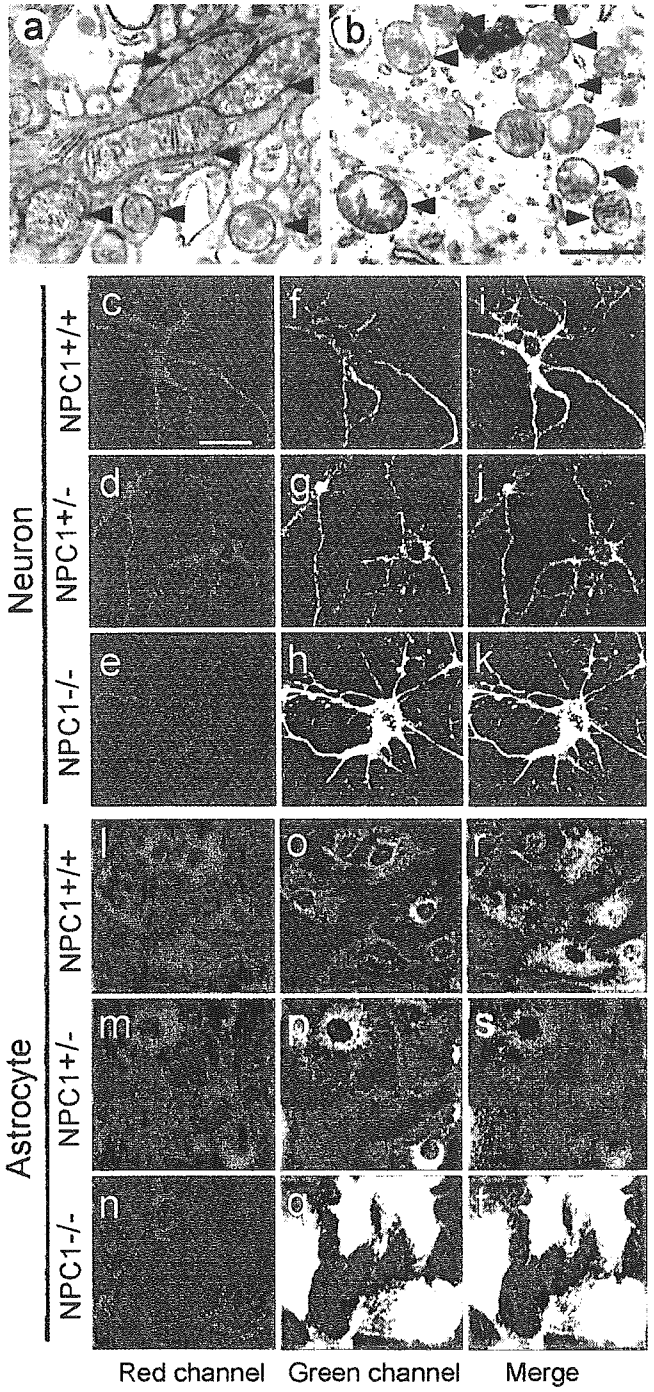

FIG. 1. **The morphology and membrane potential of mitochondria in neurons and astrocytes isolated from mouse brains.** Electron microscopy was performed on brains from NPC1+/+ (*a*) and NPC1−/− (*b*) mice at 9 weeks of age. *Arrowheads* indicate the mitochondria. *Bar* = 1 μm. The mitochondrial membrane potential for cultured neurons (*c–k*) and astrocytes (*l–t*) prepared from NPC1+/+, NPC1+/−, and NPC1−/− mouse brains was determined by staining with Mitotracker JC-1. Cells stained with JC-1 were viewed by confocal microscopy using the red channel for neurons (*c*, *d*, and *e*) and astrocytes (*l*, *m*, and *n*), whereas the green channel was used for neurons (*f*, *g*, and *h*) and astrocytes (*o*, *p*, and *q*). The merge images for neurons (*i*, *j*, and *k*) and astrocytes (*r*, *s*, and *t*) are also shown. *Bar* = 25 μm.

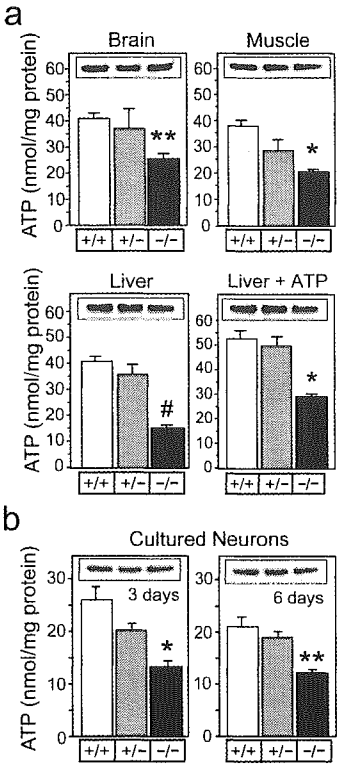

FIG. 2. **The level of ATP in mouse brain, muscle, liver, and cultured neurons.** The level of ATP was determined in brain, muscle, and liver removed from NPC1+/+, NPC1+/−, and NPC1−/− mice at 9 weeks of age (*a*). In addition, the level of ATP was also determined in liver samples for which ATP was added at a concentration of 20 nmol/mg of protein. For each of the samples, an equivalent amount of protein was used to compare the level of ATP. *, $p < 0.002$ and 0.05 *versus* NPC1+/+ and NPC1+/−, respectively. **, $p < 0.03$ *versus* NPC1+/+ and NPC1+/−. #, $p < 0.001$ *versus* NPC1+/+ and NPC1+/−. Data show mean ± S.E. of four samples. Three independent experiments show similar results. *b*, the level of ATP was determined in cultured cortical neurons prepared from NPC1+/+, NPC1+/−, and NPC1−/− mouse brains on embryonic day 16. For each of the samples, an equivalent amount of protein isolated from neurons maintained in serum-free media and harvested at days 3 and 6 in culture were used to compare the level of ATP. *, $p < 0.002$ *versus* NPC1+/+ and *, $p < 0.05$ *versus* NPC1+/−. **, $p < 0.03$ *versus* NPC1+/+ and NPC1+/−. For each of the respective tissues and cultured cortical neurons, immunoblot analysis of VDAC was used as an internal control (*a* and *b*, *inset*). The results represent the mean ± S.E. of four different samples, and are representative of three independent experiments.

mined in purified mitochondrial fractions isolated from NPC1+/+, NPC1+/−, and NPC1−/− mouse brains at 9 weeks of age. The purity of mitochondria in the P3 fraction isolated from a NPC1+/+ mouse brain was confirmed by enrichment of cytochrome *c* oxidase, and the absence of specific markers, such as lysosomal (cathepsin L), endoplasmic reticulum (Bip/GRP78), Golgi apparatus (GM130), and plasma membrane (Na^+,K^+-ATPase) markers (Fig. 3*a*). Furthermore, the purity of mitochondria in the P3 fraction isolated from a NPC1+/+ mouse brain was confirmed by electron microscopy (Fig. 3*b*). The results indicated there were no significant differences in the enzyme activities associated with complexes I + III, II + III, and IV of the different mouse brains that were analyzed (Fig. 3*c*). In contrast, the enzyme activities associated with complex V for the hydrolysis of ATP (F_1F_0-ATPase), and for the synthesis of ATP (ATP synthase), were significantly decreased in mitochondria isolated from NPC1−/− brains, compared with those from NPC1+/+ and NPC1+/− (Fig. 3*d*). These results are consistent with and explain the observation that total ATP levels are decreased in NPC1−/− tissues (Fig. 2*a*) and neurons (Fig. 2*b*). Because the synthesis of ATP is not entirely regulated by the coupling of sequential oxidation steps through the respiratory chain, but also by the mitochondrial uncoupling proteins (UCPs) (31), we also examined the amount of UCP-2 residing in the mitochondria fraction isolated from mouse brain using immunoblot analysis. The amount of UCP-2 determined

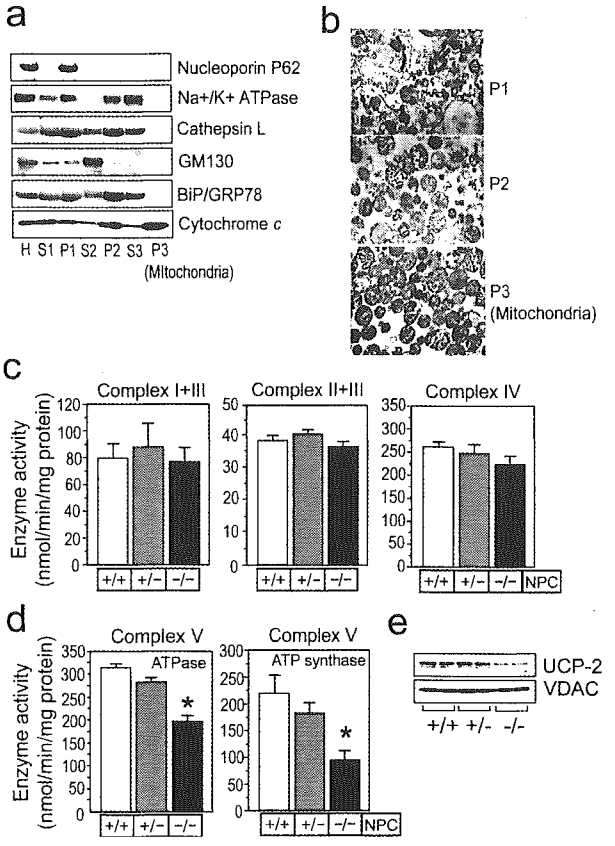

FIG. 3. **Enzymatic analysis of mitochondria complexes I + III, II + III, IV, and V using purified mitochondria from mouse brains.** The enzyme activity of mitochondria complexes I + III, II + III, IV, and V were determined in brains from NPC1+/+, NPC1+/−, and NPC1−/− mice at 9 weeks of age. The fraction containing purified brain mitochondria (*P3*), along with other cellular fractions (*P1*, *P2*, *P3*, *S1*, and *S2*), were isolated as described under "Experimental Procedures." The purity of mitochondria was confirmed by determining the distribution of specific markers such as cytochrome *c* oxidase (mitochondria), cathepsin L (lysosomal), Bip/GRP78 (endoplasmic reticulum), GM130 (Golgi apparatus), and Na^+,K^+-ATPase (plasma membrane) using immunoblot analysis (*a*). Electron microscopy (EM) analysis of P1, P2, and P3 fractions, isolated from a NPC1+/+ mouse brain was performed to demonstrate purification of mitochondria in the P3 fraction (*b*). The enzymatic analysis of complexes I + III, II + III, and IV was determined using P3 fractions isolated from brains of NPC1+/+, NPC1+/−, and NPC1−/− mice (*c*). The enzymatic analysis of complex V was determined by measuring the hydrolysis rate of ATP (ATPase), and the synthesis rate of ATP from ADP (ATP synthesis), using P3 fractions isolated from brains of NPC1+/+, NPC1+/−, and NPC1−/− mice (*d*). *, $p < 0.01$ *versus* NPC1+/+ and NPC1+/−. The results represent the mean ± S.E. of four different samples and are representative of three independent experiments. Immunoblot analysis of each representative tissue was performed using UCP-2 and immunoblot analysis of VDAC was used as an internal control (*e*).

in mitochondria isolated from the NPC1−/− brains was markedly reduced compared with that in the mitochondria from the NPC1+/− and NPC1−/− brains (Fig. 3*e*). As an internal control, immunoblot analysis was performed to determine the amount of VDAC. These results suggest that the enhanced uncoupling respiratory chain function from ATP synthesis by UCP-2 is not involved in the decreased ATP synthesis in NPC1−/− tissues, and that the expression of UCP-2 is down-regulated possibly because of a negative feedback regulation.

Because there may be a possibility that the decreased levels of ATP and ATP synthase activity are because of indirect consequences caused by neuronal death occurring at 9 weeks of age, we analyzed those parameters in younger mice at 10 days of age. Similar to the results shown in Figs. 2 and 3, the levels of ATP and ATP synthase activity in NPC1−/− brains were

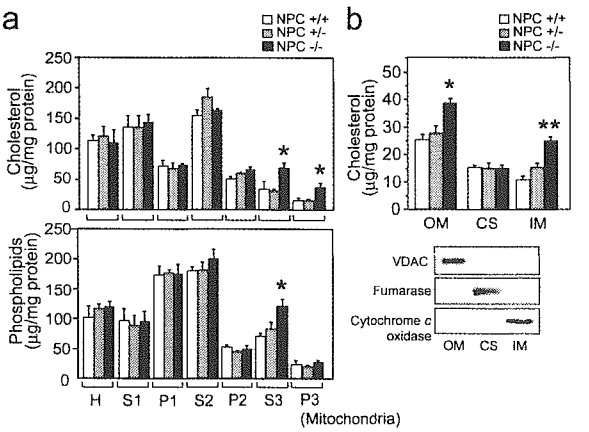

FIG. 4. **The level of cholesterol and phospholipids in cellular fractions and purified mitochondria.** The level of cholesterol and phospholipids in cellular fractions and purified mitochondria was determined in NPC1+/+, NPC1+/−, and NPC1−/− mouse brains (*a*). The level of cholesterol in the OM, CS, and the IM was determined for purified mitochondria (*P3*). The distribution of specific markers for OM (*VDAC*), CS (*fumarase*), and IM (*cytochrome c oxidase*) was determined using immunoblot analysis, and used to verify purification of the respective mitochondria membranes (*b*). *, $p < 0.0001$ and **, $p < 0.005$ *versus* NPC1+/+ and NPC1+/−. The results represent the mean ± S.E. of four different samples and are representative of three independent experiments.

significantly decreased compared with those in NPC1+/+ brains, and the cholesterol level was increased in the mitochondria that were isolated from brains of NPC1−/− mice (see Supplemental Materials, Fig. S1).

The Level of Cholesterol and Phospholipids in Cellular Fractions and Purified Mitochondria—Because the most prominent feature of NPC1−/− cells is altered cholesterol metabolism, the concentration of cholesterol and phospholipids in cellular fractions and purified mitochondria fraction (P3) was determined in NPC1+/+, NPC1+/−, and NPC1−/− mouse brains. The results indicated that the concentration of cholesterol was significantly increased in fractions S3 (enriched with plasma membrane, lysosome, and endoplasmic reticulum), and P3 (mitochondria), whereas the concentration of phospholipids was increased only in fraction S3 (Fig. 4*a*). This result would therefore exclude the possibility that contamination of lipid between fractions S3 and P3 had occurred. In addition, the concentration of cholesterol was determined for specific membranes purified from mitochondria, specifically the OM, CS, and IM. The results indicated that the concentration of cholesterol was significantly increased in both the OM and IM of mitochondria isolated from NPC1−/− mouse brains, compared with the same membranes of mitochondria isolated from NPC1+/+ and NPC1+/− mouse brains (Fig. 4*b*, *upper panel*). The purity of specific membranes purified from mitochondria was examined and confirmed using immunoblot analysis for proteins associated with the OM (VDAC), CS (fumarase, a matrix marker), and IM (cytochrome *c* oxidase) (Fig. 4*b*, *lower panel*).

Kinetic Analysis of Cholesterol and PC Transport to and from Mitochondria—Kinetic analysis of cholesterol transport to mitochondria, which was exogenously added as [^{14}C]cholesterol-labeled HDL or endogenously synthesized [^{14}C]cholesterol, was determined using astrocytes prepared from NPC1+/+, NPC1+/−, and NPC1−/− mouse brains. As indicated in Fig. 5*a*, [^{14}C]cholesterol-labeled HDL added to cells was transported into the cell homogenate and mitochondria at a higher rate in NPC1−/− cells than NPC1+/+ and NPC1+/− cells at 12 h. Similarly, the amount of [^{14}C]PC transported into NPC1−/− cells (homogenate) was at a higher rate than NPC1+/+ and NPC1+/− cells at 8 and 12 h (Fig. 5*b*). However,

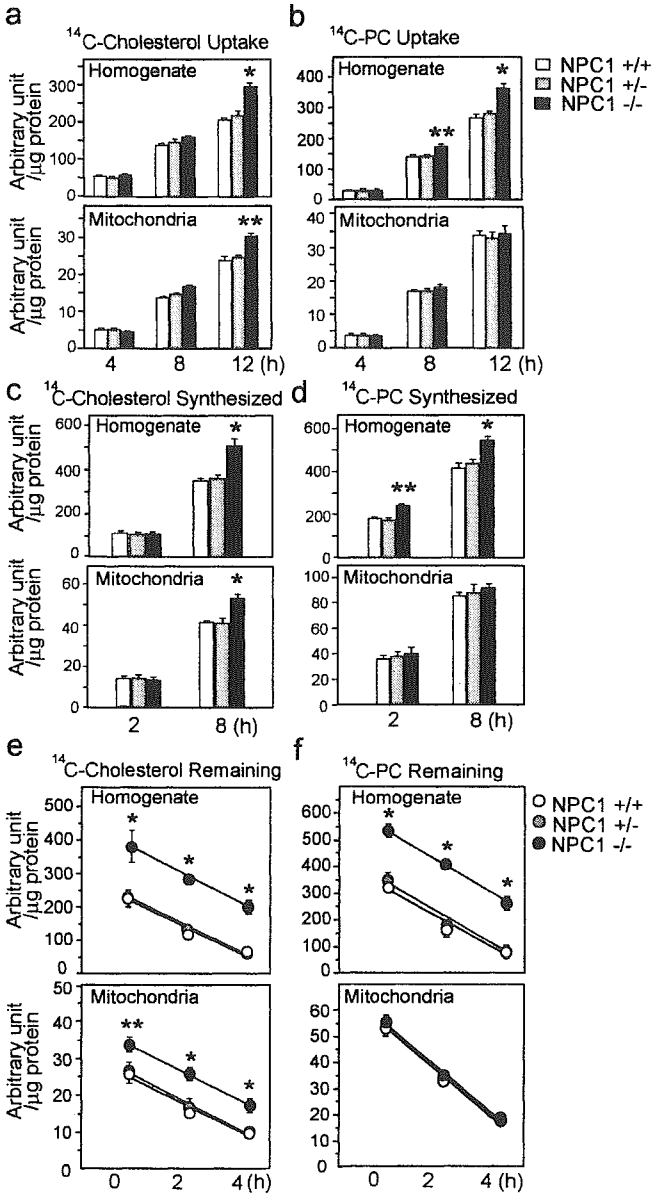

FIG. 5. **Kinetic analysis of cholesterol and PC transport to and from mitochondria.** Kinetic analysis of cholesterol and PC transport to and from mitochondria was performed using astrocytes isolated from NPC1+/+, NPC1+/−, and NPC1−/− mice. The astrocytes prepared from the brains of wild type mice were labeled with [^{14}C]acetate, and HDL containing [^{14}C]cholesterol and [^{14}C]PC was isolated as described under "Experimental Procedures." The astrocytes prepared from the brains of NPC1+/+, NPC1+/−, and NPC1−/− mice were incubated with an equivalent amount of HDL (1 μg of cholesterol/ml), and the amount of [^{14}C]cholesterol (*a*) and [^{14}C]PC (*b*) transported into the cells and mitochondria were determined. *, $p < 0.001$ and **, $p < 0.05$ *versus* NPC1+/+ and NPC1+/−. The amount of endogenously synthesized cholesterol (*c*) and PC (*d*) in the cell homogenate and transported to mitochondria was determined. *, $p < 0.001$ and **, $p < 0.01$ *versus* NPC1+/+ and NPC1+/−. The amount of lipid removed from astrocytes, and mitochondria isolated from astrocytes, was determined using astrocytes cultures prepared from NPC1+/+, NPC1+/−, and NPC1−/− mouse brains as described under "Experimental Procedures." The levels of [^{14}C]cholesterol (*e*) and [^{14}C]PC (*f*) remaining in the cells and mitochondria were determined after 0, 2, and 4 h of incubation with labeled HDL. *, $p < 0.0001$ and **, $p < 0.002$ *versus* NPC1+/+ and NPC1+/−. For studies *a–f*, the results indicate the mean ± S.E. of four samples, and are representative of two independent experiments.

there was no significant difference in the transport of exogenously added PC into mitochondria among the three genotypes (Fig. 5*b*, *lower panel*). The level of endogenously synthesized cholesterol and PC in the homogenate and that transported into mitochondria were also determined. The results indicated that there was a higher rate of synthesis of cholesterol and PC in NPC1−/− cells (homogenate) compared with NPC1+/+ and NPC1+/− cells (Fig. 5, *c* and *d*). However, although the transport of endogenously synthesized cholesterol into mitochondria of NPC1−/− cells was higher than NPC1+/+ and NPC1+/− cells, there was no significant difference in the transport of endogenously synthesized PC into mitochondria among the three genotypes (Fig. 5, *c* and *d*, *lower panels*).

Next, the kinetics of cholesterol and PC removal from cells and mitochondria were determined. The results indicated that the amount of [^{14}C]cholesterol remaining in the cell homogenate and mitochondria decreased with time, however, the amount of [^{14}C]cholesterol in the cell homogenate and mitochondria of NPC1−/− cells was significantly higher compared with NPC1+/+ and NPC1+/− cells at every time point examined (Fig. 5*e*). In contrast, there was no difference in the level of remaining [^{14}C]PC in mitochondria among the three genotypes (Fig. 5*f*, *lower panel*). The rates of cholesterol removal calculated from the data shown in Fig. 5*e* are 40.5, 42.5, and 42.8 (arbitrary unit/h/μg of protein) from cells (homogenate), and 4.0, 4.1, and 4.3 (arbitrary unit/h/μg of protein) from mitochondria of NPC1+/+, NPC1+/−, and NPC1−/− cells, respectively, indicating that the rate of cholesterol removal is not adversely affected in NPC1−/− cells.

An Increase in the Level of Mitochondria Membrane Cholesterol Inhibits ATP Synthase—To determine whether an increase in mitochondrial cholesterol adversely affects mitochondria function, the activity of ATP synthase was determined in relation to the amount of cholesterol associated with mitochondria isolated from NPC1+/+ and NPC1−/− mouse brains. To perform this study, the hydrophilic cholesterol-sequestering agent, methyl-β-cyclodextrin, was used to remove cholesterol from mitochondria membranes. After incubation of mitochondria with 7.5 mM methyl-β-cyclodextrin, results indicated that the level of cholesterol associated with NPC1−/− mitochondria, which was significantly increased compared with NPC1+/+ mitochondria, was reduced to a level similar to that of NPC1+/+ mitochondria (Fig. 6*b*). In accordance with this decrease in the level of cholesterol associated with NPC1−/− mitochondria, the activity of ATP synthase was significantly increased to a level similar to that of NPC1+/+ mitochondria (Fig. 6*a*). Importantly, when the decreased cholesterol level in NPC1−/− mitochondria induced by incubation with methyl-β-cyclodextrin was recovered by the subsequent incubation with 50 μM cholesterol (Fig. 6*b*, *right panel*), the enhanced ATP synthase activity induced by methyl-β-cyclodextrin was reduced to a level similar to that of nontreated NPC1−/− mitochondria (Fig. 6*a*, *right panel*). In addition, the results using NPC1+/+ mitochondria indicate that when the cholesterol level in the mitochondria was increased or decreased, the activity of ATP synthase was reduced in either case (Fig. 6, *a* and *b*, *left panels*), suggesting that there is an optimal level of cholesterol in the mitochondrial membrane for ATP synthase.

Impaired Neuronal Outgrowth in NPC1−/− Neurons Is Restored by ATP Treatment in Culture—Because ATP is required for the development of neurons (32), the effect of NPC1 deficiency on neurite outgrowth was investigated using neurons prepared from cerebral cortices derived from NPC1+/+, NPC1+/−, and NPC1−/− mouse brains. Using immunocytochemistry, the staining neurons for β-tubulin indicated that while neurite extension was clearly evident at 72 h in NPC1+/+ and NPC1+/− neurons, it was impaired in NPC1−/− neurons (Fig. 7*A*, *a*, *c*, and *e*). In addition, the time-dependent analysis of neurite outgrowth indicated that neurite

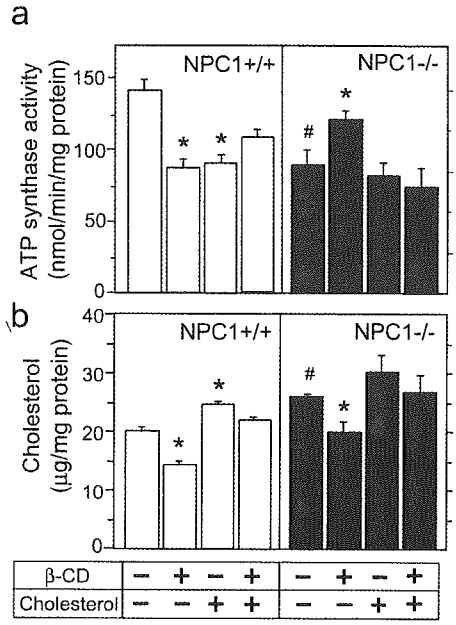

FIG. 6. **Modulation of ATP synthase activity by cholesterol in the mitochondrial membrane.** The activity of ATP synthase was determined in relation to the level of cholesterol associated with mitochondria isolated from NPC1+/+ and NPC1−/− mouse brains. The brain P2 fractions isolated from another these mouse brains was incubated in the presence of methyl-β-cyclodextrin (β-CD) (7.5 mM) or cholesterol (50 μM) for 20 min at 37 °C, followed by centrifugation to isolate mitochondria (P3). For β-CD and cholesterol treatment, the P2 fraction was incubated with β-CD, rinsed, and then incubated with cholesterol for 20 min at 37 °C, followed by centrifugation to isolate mitochondria. The activity of ATP synthase per mitochondrial protein (*top panel*) and the concentration of cholesterol (*bottom panel*) associated with the purified mitochondria were determined as described under "Experimental Procedures." *, $p < 0.02$ *versus* control (nontreatment); #, $p < 0.01$ *versus* NPC1+/+ control. The results represent the mean ± S.E. of three different samples and are representative of three independent experiments.

extension and sprouting were significantly suppressed in NPC1−/− neurons, compared with NPC1+/+ and NPC1+/− neurons (Fig. 7*B*, *a* and *c*). Importantly, both the neurite length and number were restored upon addition of 0.5 mM ATP (Fig. 7, *A*, *f*, and *B*, *b* and *d*). We have confirmed that ATP added extracellularly remains in the medium and increased cellular ATP levels for at least 24 h (see Supplemental Materials, Fig. S2). Next, the effect of nucleotides other than ATP, such as ADP and AMP-PNP, on neurite outgrowth was determined. The results indicated that ADP added extracellularly had no significant effect on neurite outgrowth (number and length) in both NPC1+/+ and NPC1−/− neurons (Fig. 7*C*, *c* and *d*). In contrast, as has been reported previously (33), the nonhydrolyzable analogue, AMP-PNP, inhibited neurite outgrowth in NPC1+/+ neurons (Fig. 7*C*, *c* and *d*). The levels of ATP in cultured neurons in the absence or presence of ATP, ADP, or AMP-PNP were determined. Only the addition of ATP increased the cellular level of ATP (Fig. 7*C*, *a*). These results indicate that deterioration of neurite outgrowth, which is present in NPC1−/− neurons, results from a decreased level of ATP.

DISCUSSION

The molecular mechanism responsible for neurodegeneration in NPC1 disease remains undetermined. The present study describes severe mitochondrial abnormalities that may be responsible for causing impaired neuronal function and neurodegeneration in NPC1−/− mouse brains. The results from this study strongly suggest that neuronal dysfunctions and degeneration in NPC1−/− mouse brains arise from (i) a decrease in mitochondrial membrane potential, (ii) a decrease in ATP synthesis, and (iii) a decrease in the level of cellular ATP. In addition, NPC1−/− neurons exhibited impaired neurite outgrowth, which was restored by the addition of ATP to the culture media. Each of the abnormalities identified in mitochondria of NPC1−/− neurons was associated with an elevation in the cholesterol concentration of mitochondria membranes, and that by reducing the cholesterol concentration of mitochondria membranes, ATP synthase activity was restored to normal.

The results demonstrated that an increase in the level of mitochondria membrane cholesterol impaired mitochondrial function. Additional support for cholesterol being the offending metabolite was confirmed by incubating the water-soluble cholesterol sequestering agent, methyl-β-cyclodextrin, in the presence of NPC1−/− mitochondria membranes to reduce membrane cholesterol. This reduced NPC1−/− mitochondria membrane cholesterol to a level that was similar to NPC1+/+ mitochondria membranes, and enhanced ATP synthase activity. In addition, the recovering cholesterol level in the methyl-β-cyclodextrin-treated mitochondria by subsequent incubation with cholesterol decreased ATP synthase activity to an initial level. The increased molar ratio of cholesterol to phospholipids measured in NPC1−/− mitochondria membranes suggests that the basic structure and/or physical property of the mitochondria membrane is adversely affected, and that the altered physical properties of these membranes leads to a reduced proton motive force and membrane potential, which in turn decreases ATP synthesis. In support of this result, previous studies have demonstrated that an elevation of cholesterol concentration in the inner mitochondrial membrane reduces mitochondrial membrane potential, induces mitochondria depolarization and uncoupling responsible for oxidative phosphorylation, and henceforth impairing ATP synthesis (34–36). Each of these defects was also observed in NPC1−/− brains and neurons. As a result, it is possible that an increased level of cholesterol within mitochondria membranes, known to adversely influence membrane fluidity (36), leads to impaired mitochondria permeability transition, mitochondrial membrane potential, and ATP synthesis in NPC1−/− cells. Interestingly, the fact that methyl-β-cyclodextrin treatment also reduced ATP synthesis in NPC1+/+ mitochondria membranes suggests that there is an optimal ratio of cholesterol to phospholipids in mitochondria membranes for ATP synthesis.

Although the NPC1 protein has been shown to facilitate the transport of cholesterol from late endosomes/lysosomes to the trans-Golgi network, the plasma membrane, and the endoplasmic reticulum, the results of this study show that exogenously added cholesterol and endogenously synthesized cholesterol are transported into mitochondria in NPC1-deficient astrocytes. These results suggest the existence of a cholesterol transport pathway independent of the NPC1 protein. The results also suggest that while the cholesterol level in mitochondrial membranes is elevated in NPC1−/− neurons, the phospholipid level in these mitochondria membranes is similar to NPC1+/+ neurons. Finally, because the mitochondria were shown not to be contaminated by late endosomes/lysosomes using both immunoblot analysis and electron microscopy, these results suggest that cholesterol metabolism with respect to the mitochondria may be independently affected in NPC1−/− cells. It is unclear why the level of cholesterol in mitochondrial membranes increases in NPC1−/− brains, although accumulation of cholesterol in late endosome/lysosome and the increased level of *de novo* synthesis of cholesterol in NPC1−/− cells may somehow contribute to increased cholesterol transport to the mitochondrial membranes.

The similar cholesterol removal rate from mitochondria in

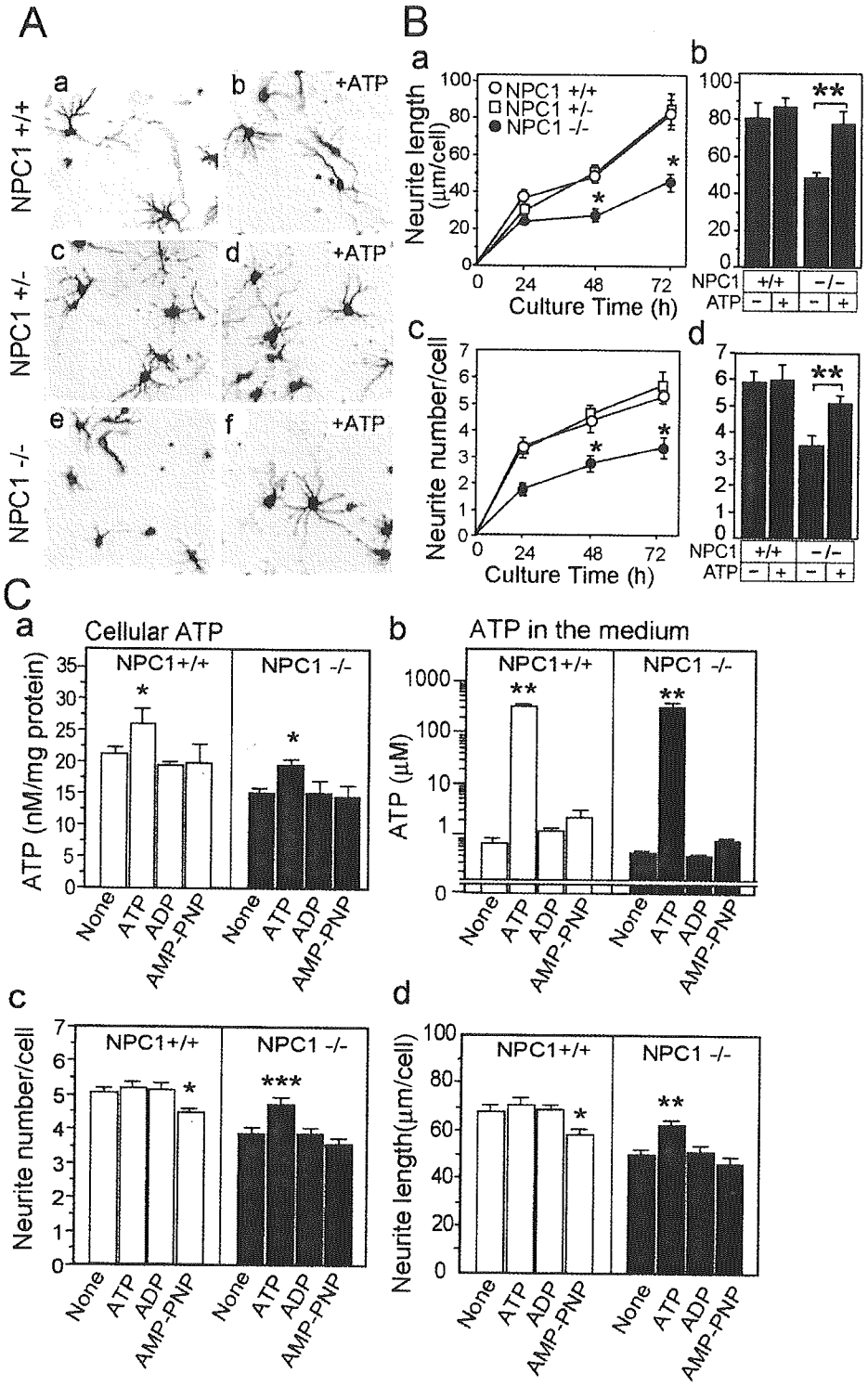

FIG. 7. **Effect of NPC1 deficiency on neurite outgrowth.** The effect of NPC1 deficiency on neurite outgrowth was investigated using neurons prepared from cerebral cortices derived from NPC1+/+, NPC1+/−, and NPC1−/− mouse brains. *A*, neurons prepared from cerebral cortices of NPC1+/+ (*a* and *b*), NPC1+/− (*c* and *d*), and NPC1−/− (*e* and *f*) were cultured in serum-free medium for 72 h, then fixed and stained for β-tubulin. *B*, neurite length/cell (*a*) and neurite number/cell (*c*) were determined as a function of time as described under "Experimental Procedures." The effect of incubating neurons in media supplemented with 0.5 mM ATP for 72 h and measuring neurite extension (*b*) and sprouting (*d*) was determined. *, $p < 0.005$ *versus* NPC1+/+ and NPC1+/− and **, $p < 0.02$. *C*, neurons prepared from cerebral cortices of NPC1+/+ and NPC1−/− mouse brains were incubated with none, ATP (0.5 mM), ADP (0.5 mM), or AMP-PNP (0.5 mM) in serum-free medium for 72 h. The cultures and the media were then harvested and the levels of cellular ATP (*a*), ATP remaining in the media (*b*), neurite length/cell (*c*), and neurite number/cell (*d*) of each treatment were determined. *, $p < 0.05$, **, $p < 0.001$, and ***, $p < 0.02$ *versus* others. These data represent the mean ± S.E. of 80 cells from each genotype and are representative of three independent experiments.

NPC1+/+, NPC1+/−, and NPC1−/− cells suggested that the elevated cholesterol level in NPC1−/− mitochondria may be because of increased cholesterol transport to mitochondria. Several mechanisms have been proposed for phospholipid transport between the mitochondria and other biological membranes (37, 38). However, cholesterol transport to and from the

mitochondria is largely unknown. The results of this study suggest that NPC1 may also modulate cholesterol transport to mitochondria, in addition to the role of NPC1 in cholesterol transport to the trans-Golgi network, the plasma membrane, and the endoplasmic reticulum (39). Unlike these cellular compartments that become relatively cholesterol-deficient when NPC1 is defective (positive regulation), mitochondria become relatively cholesterol-enriched (negative regulation). Such a mechanism proposed for the function of NPC1 would be consistent with cholesterol serving as the offending metabolite, as it adversely affects critical functions required for mitochondria.

Importantly, it is well established that mitochondria contribute to steroidogenesis. The late-limiting step in steroidogenesis involves the conversion of cholesterol into pregnenolone by cytochrome $P450_{scc}$ and its associated electron-transport chain, which are known to be associated with the inner membrane of mitochondria (40). In an elegant study recently performed by Griffin *et al.* (22) it was determined that decreased levels of neurosteroids may actually be the cause of neurodegeneration in NPC1−/− mice. However, it must be emphasized that the mechanism responsible for the loss in neurosteroids and neurosteroidogenic activity remains undefined. Because mitochondria obviously have a critical role in steroidogenesis, the altered function of mitochondria described in the present study is consistent with this organelle having a key role in promoting neurodegeneration.

Recently, there has been evidence suggesting similarities in tauopathy between NPC disease and Alzheimers disease (AD). The brains of NPC patients have been shown to have neurofibrillary tangles and neurodegeneration without amyloid β-protein (Aβ) deposits (13), which is believed to be responsible for promoting pathologies typically associated AD. The presence of neurofibrillary tangles is one of the diagnostic hallmarks of AD, and a major component of neurofibrillary tangles is hyperphosphorylated tau. Interestingly, Aβ adversely affects cellular cholesterol metabolism (23, 41), which in turn, induces tau phosphorylation in cultured neurons (42). The altered cholesterol metabolism in NPC1−/− brains and cells has also been shown to induce tau phosphorylation in NPC1−/− brains and cells (5, 19). Moreover, it has now been established that altered cholesterol metabolism is associated with the development of AD (43, 44), and that mitochondrial dysfunction is involved in the development of AD (45, 46). Therefore, it may be possible that AD and NPC share a common pathway involving cholesterol metabolism leading to neurodegeneration via mitochondrial dysfunction (44).

In conclusion, the present study has demonstrated that an elevation in the level of mitochondria membrane cholesterol, because of deficient NPC1 protein function, decreases cellular ATP levels causing impaired neurite outgrowth and enhanced susceptibility to oxygen radicals, which in turn is supposed to promote neurodegeneration in NPC1−/− mice. The addition of ATP can restore impaired neurite outgrowth and high susceptibility to neurotoxicity, which supports this notion. This information, suggesting that severe mitochondrial dysfunctions and subsequent decrease in cellular ATP levels may be the cause of neurodegeneration in NPC1 disease, provides a novel insight and direction for pursuing viable treatment options for NPC1 disease.

Acknowledgment—We thank Hitoshi Yamashita for helpful discussion.

REFERENCES

1. Patterson, M. C., Vanier, M. T., Suzuki, K., Morris, J. A., Carstea, E. D., Neufeld, E. B., Blanchette Mackie, E. J., and Pentchev, P. G. (2001) in *The Metabolic and Molecular Basis of Inherited Disease* (Scriver, C. R., Beaudet, A. L., Sly, W. S., and Valle, D., eds) pp. 3611–3633, McGraw-Hill Inc., New York
2. Liscum, L., Ruggiero, R. M., and Faust, J. R. (1989) *J. Cell Biol.* **108,** 1625–1636
3. Pentchev, P. G., Kruth, H. S., Comly, M. E., Butler, J. D., Vanier, M. T., Wenger, D. A., and Patel, S. (1986) *J. Biol. Chem.* **261,** 16775–16780
4. Kobayashi, T., Beuchat, M. H., Lindsay, M., Frias, S., Palmiter, R. D., Sakuraba, H., Parton, R. G., and Gruenberg, J. (1999) *Nat. Cell Biol.* **1,** 113–118
5. Sawamura, N., Gong, J. S., Garver, W. S., Heidenreich, R. A., Ninomiya, H., Ohno, K., Yanagisawa, K., and Michikawa, M. (2001) *J. Biol. Chem.* **276,** 10314–10319
6. Ribeiro, I., Marcao, A., Amaral, O., Sa Miranda, M. C., Vanier, M. T., and Millat, G. (2001) *Hum. Genet.* **109,** 24–32
7. Loftus, S. K., Morris, J. A., Carstea, E. D., Gu, J. Z., Cummings, C., Brown, A., Ellison, J., Ohno, K., Rosenfeld, M. A., Tagle, D. A., Pentchev, P. G., and Pavan, W. J. (1997) *Science* **277,** 232–235
8. Carstea, E. D., Morris, J. A., Coleman, K. G., Loftus, S. K., Zhang, D., Cummings, C., Gu, J., Rosenfeld, M. A., Pavan, W. J., Krizman, D. B., Nagle, J., Polymeropoulos, M. H., Sturley, S. L., Ioannou, Y. A., Higgins, M. E., Comly, M., Cooney, A., Brown, A., Kaneski, C. R., Blanchette-Mackie, E. J., Dwyer, N. K., Neufeld, E. B., Chang, T. Y., Liscum, L., Strauss, J. F., III, Ohno, K., Zeigler, M., Carmi, R., Sokol, J., Markie, D., O'Neill, R. R., van Diggelen, O. P., Elleder, M., Patterson, M. C., Brady, R. O., Vanier, M. T., Pentchev, P. G., and Tagle, D. A. (1997) *Science* **277,** 228–231
9. Liscum, L., and Klansek, J. J. (1998) *Curr. Opin. Lipidol.* **9,** 131–135
10. Neufeld, E. B., Wastney, M., Patel, S., Suresh, S., Cooney, A. M., Dwyer, N. K., Roff, C. F., Ohno, K., Morris, J. A., Carstea, E. D., Incardona, J. P., Strauss, J. F., 3rd, Vanier, M. T., Patterson, M. C., Brady, R. O., Pentchev, P. G., and Blanchette-Mackie, E. J. (1999) *J. Biol. Chem.* **274,** 9627–9635
11. Garver, W. S., Heidenreich, R. A., Erickson, R. P., Thomas, M. A., and Wilson, J. M. (2000) *J. Lipid Res.* **41,** 673–687
12. Wojtanik, K. M., and Liscum, L. (2003) *J. Biol. Chem.* **278,** 14850–14856
13. Suzuki, K., Parker, C. C., Pentchev, P. G., Katz, D., Ghetti, B., D'Agostino, A. N., and Carstea, E. D. (1995) *Acta Neuropathol.* **89,** 227–238
14. Love, S., Bridges, L. R., and Case, C. P. (1995) *Brain* **118,** 119–129
15. Auer, I. A., Schmidt, M. L., Lee, V. M., Curry, B., Suzuki, K., Shin, R. W., Pentchev, P. G., Carstea, E. D., and Trojanowski, J. Q. (1995) *Acta Neuropathol.* **90,** 547–551
16. Morris, M. D., Bhuvaneswaran, C., Shio, H., and Fower, S. (1982) *Am. J. Pathol.* **108,** 140–149
17. Higashi, Y., Murayama, S., Pentchev, P. G., and Suzuki, K. (1993) *Acta Neuropathol.* **85,** 175–184
18. Bu, B., Li, J., Davies, P., and Vincent, I. (2002) *J. Neurosci.* **22,** 6515–6525
19. Sawamura, N., Gong, J. S., Chang, T. Y., Yanagisawa, K., and Michikawa, M. (2003) *J. Neurochem.* **84,** 1086–1096
20. Walkley, S. U., Siegel, D. A., Dobrenis, K., and Zervas, M. (1998) *Ann. N. Y. Acad. Sci.* **845,** 188–199
21. Liu, Y., Wu, Y. P., Wada, R., Neufeld, E. B., Mullin, K. A., Howard, A. C., Pentchev, P. G., Vanier, M. T., Suzuki, K., and Proia, R. L. (2000) *Hum. Mol. Genet.* **9,** 1087–1092
22. Griffin, L. D., Gong, W., Verot, L., and Mellon, S. H. (2004) *Nat. Med.* **10,** 704–711
23. Michikawa, M., Gong, J. S., Fan, Q. W., Sawamura, N., and Yanagisawa, K. (2001) *J. Neurosci.* **21,** 7226–7235
24. Gong, J. S., Kobayashi, M., Hayashi, H., Zou, K., Sawamura, N., Fujita, S. C., Yanagisawa, K., and Michikawa, M. (2002) *J. Biol. Chem.* **277,** 29919–29926
25. Schnaitman, C., and Greenawalt, J. W. (1968) *J. Cell Biol.* **38,** 158–175
26. Wang, X., Liu, Z., Eimerl, S., Timberg, R., Weiss, A. M., Orly, J., and Stocco, D. M. (1998) *Endocrinology* **139,** 3903–3912
27. Sottocasa, G. L., Kuylenstierna, B., Ernster, L., and Bergstrand, A. (1967) *J. Cell Biol.* **32,** 415–438
28. Trumpower, B. L., and Edwards, C. A. (1979) *J. Biol. Chem.* **254,** 8697–8706
29. Zheng, X., Shoffner, J. M., Lott, M. T., Voljavec, A. S., Krawiecki, N. S., Winn, K., and Wallace, D. C. (1989) *Neurology* **39,** 1203–1209
30. Salvioli, S., Ardizzoni, A., Franceschi, C., and Cossarizza, A. (1997) *FEBS Lett.* **411,** 77–82
31. Ricquier, D., Casteilla, L., and Bouillaud, F. (1991) *FASEB J.* **5,** 2237–2242
32. Mattson, M. P., and Partin, J. (1999) *J. Neurosci. Res.* **56,** 8–20
33. Skladchikova, G., Ronn, L. C., Berezin, V., and Bock, E. (1999) *J. Neurosci. Res.* **57,** 207–218
34. Calanni Rindina, F., Baracca, A., Solaini, G., Rabbi, A., and Parenti Castelli, G. (1986) *FEBS Lett.* **198,** 353–356
35. Yao, P. M., and Tabas, I. (2001) *J. Biol. Chem.* **276,** 42468–42476
36. Colell, A., Garcia-Ruiz, C., Lluis, J. M., Coll, O., Mari, M., and Fernandez-Checa, J. C. (2003) *J. Biol. Chem.* **278,** 33928–33935
37. Shiao, Y. J., Lupo, G., and Vance, J. E. (1995) *J. Biol. Chem.* **270,** 11190–11198
38. Kuge, O., and Nishijima, M. (2003) *J. Biochem. (Tokyo)* **133,** 397–403
39. Garver, W. S., Krishnan, K., Gallagos, J. R., Michikawa, M., Francis, G. A., and Heidenreich, R. A. (2002) *J. Lipid Res.* **43,** 579–589
40. Garren, L. D., Gill, G. N., Masui, H., and Walton, G. M. (1971) *Recent Prog. Horm. Res.* **27,** 433–478
41. Gong, J. S., Sawamura, N., Zou, K., Sakai, J., Yanagisawa, K., and Michikawa, M. (2002) *J. Neurosci. Res.* **70,** 438–446
42. Fan, Q. W., Yu, W., Senda, T., Yanagisawa, K., and Michikawa, M. (2001) *J. Neurochem.* **76,** 391–400
43. Simons, M., Keller, P., Dichgans, J., and Schulz, J. B. (2001) *Neurology* **57,** 1089–1093
44. Michikawa, M. (2003) *J. Neurosci. Res.* **72,** 141–146
45. Hirai, K., Aliev, G., Nunomura, A., Fujioka, H., Russell, R. L., Atwood, C. S., Johnson, A. B., Kress, Y., Vinters, H. V., Tabaton, M., Shimohama, S., Cash, A. D., Siedlak, S. L., Harris, P. L., Jones, P. K., Petersen, R. B., Perry, G., and Smith, M. A. (2001) *J. Neurosci.* **21,** 3017–3023
46. Lustbader, J. W., Cirilli, M., Lin, C., Xu, H. W., Takuma, K., Wang, N., Caspersen, C., Chen, X., Pollak, S., Chaney, M., Trinchese, F., Liu, S., Gunn-Moore, F., Lue, L. F., Walker, D. G., Kuppusamy, P., Zewier, Z. L., Arancio, O., Stern, D., Yan, S. S., and Wu, H. (2004) *Science* **304,** 448–452

0013-7227/05/$15.00/0
Printed in U.S.A.

Endocrinology 146(8):3286–3294

doi: 10.1210/en.2005-0043

Deficiency of the Very Low-Density Lipoprotein (VLDL) Receptors in Streptozotocin-Induced Diabetic Rats: Insulin Dependency of the VLDL Receptor

Tadao Iwasaki,* Sadao Takahashi,* Masao Takahashi, Yasuo Zenimaru, Takeshi Kujiraoka, Mitsuaki Ishihara, Makoto Nagano, Jinya Suzuki, Isamu Miyamori, Hironobu Naiki, Juro Sakai, Takahiro Fujino, Norman E. Miller, Tokuo T. Yamamoto, and Hiroaki Hattori

Department of Advanced Medical Technology and Development, BML, Inc. (T.I., T.K., M.I., M. N., H.H.), Kawagoe 50-1101, Japan; Third Department of Internal Medicine, Faculty of Medical Sciences (S.T., Y.Z., J.Su., I. M.), and Second Department of Pathology (H. N.), University of Fukui, Fukui 910-1193, Japan; Department of Cardiovascular Surgery, Hiratsuka Kyosai Hospital (M.T.), Hiratsuka 254-8502, Japan; Laboratory for Systems Biology and Medicine, Research Center for Advanced Science and Technology, University of Tokyo (J.Sa.), Komaba 153-8904, Japan; Exploratory Research for Advanced Technology of Japan Science and Technology Corp. (J.Sa.), Aomi 135-0064, Japan; Department of Bioscience, Integrated Center for Science, Ehime University (T.F.), Shigenobu 791-0295, Japan; Department of Cardiovascular Biochemistry, St. Barts and the Royal London School of Medicine (N.E.M.), London EC1A 7BE, United Kingdom; and Center for Advanced Genome Research, Institute of Aging, Development, and Cancer, Tohoku University (T.T.Y.), Sendai 981-8555, Japan

Hyperlipidemia is a common feature of diabetes and is related to cardiovascular disease. The very low-density lipoprotein receptor (VLDL-R) is a member of the low-density lipoprotein receptor (LDL-R) family. It binds and internalizes triglyceride-rich lipoproteins with high specificity. We examined the etiology of hyperlipidemia in the insulin-deficient state. VLDL-R expression in heart and skeletal muscle were measured in rats with streptozotocin (STZ)-induced diabetes. STZ rats showed severe hyperlipidemia on d 21 and 28, with a dramatic decline in VLDL-R protein in skeletal muscle (>90%), heart (~50%) and a loss of adipose tissues itself on d 28. The reduction of VLDL-R protein in skeletal muscle could not be explained simply by a decrease at the transcriptional level, because a dissociation between VLDL-R protein and mRNA expression was observed. The expression of LDL-R and LDL-R-related protein in liver showed no consistent changes. Furthermore, no effect on VLDL-triglyceride production in liver was observed in STZ rats. A decrease in postheparin plasma lipoprotein lipase activity started on d 7 and continued to d 28 at the 50% level even though severe hyperlipidemia was detected only on d 21 and 28. In rat myoblast cells, serum deprivation for 24 h induced a reduction in VLDL-R proteins. Insulin (10^{-6} M), but not IGF-I (10 ng/ml), restored the decreased VLDL-R proteins by serum deprivation. These results suggest that the combination of VLDL-R deficiency and reduced plasma lipoprotein lipase activity may be responsible for severe hyperlipidemia in insulin-deficient diabetes. (*Endocrinology* 146: 3286–3294, 2005)

IN DIABETES MELLITUS, hyperlipidemia is often observed as a result of impaired insulin action (1, 2), and their causal relations to macrovascular disease and diabetic macroangiopathy have been discussed (3). For the insulin-deficient diabetic model, streptozotocin (STZ)-induced diabetic rats (STZ rats) have been used for the study of diabetic hyperlipidemia (4–14). Several mechanisms of diabetic hyperlipidemia in STZ rats have been proposed, including increased intestinal absorption of dietary cholesterol (10–14), increased very low-density lipoprotein (VLDL) production in liver at an early period after STZ treatment (4), and decreased removal of VLDL-triglyceride (TG) from the circulation (4, 5). Lipoprotein lipase (LPL) hydrolyzes circulating TG, leading to the release of free fatty acids (FFAs), which are stored as TG in adipose tissue and serve as energy sources in skeletal muscle and heart (15). Several studies have measured LPL activity in skeletal muscle and heart in insulin-deficient diabetic animal models. Decreased activity (7, 9, 16), no change in activity (5, 17), and increased activity (6, 8) all have been observed. Variations in LPL activity probably contribute to the abnormalities in lipoprotein metabolism and the duration of the diabetic state. Recently, it has been reported that intestinal acyl-coenzyme A:cholesterol acyltransferase (ACAT-2), microsomal triglyceride transfer protein (MTP), and ATP-binding cassette transporter (ABCG5/G8) are also related to hyperlipidemia in STZ rats (12–14). However, the precise mechanisms of insulin-deficient diabetic hyperlipidemia are unclear.

The VLDL receptor (VLDL-R) is a member of the low-

First Published Online May 5, 2005

* T.I. and S.T. contributed equally to this work.

Abbreviations: ABC, ATP-binding cassette transporter; ACAT, acyl-coenzyme A:cholesterol acyltransferase; apo, apolipoprotein; FA, fatty acid; FFA, free fatty acid; GAPDH, glyceraldehyde-3-phosphate dehydrogenase; HDL, high-density lipoprotein; LDL, low-density lipoprotein; LPL, lipoprotein lipase; LRP, low-density lipoprotein receptor-related protein; MTP, microsomal triglyceride transfer protein; RAP, receptor-associated protein; SD, Sprague Dawley; STZ, streptozotocin; TC, total cholesterol; TG, triglyceride; TGPR, triglyceride production rate; VLDL, very low-density lipoprotein; β-VLDL, β-migrating very low-density lipoproteins.

Endocrinology **is published monthly by The Endocrine Society (http://www.endo-society.org), the foremost professional society serving the endocrine community.**

density lipoprotein (LDL) receptor (LDL-R) family and is most abundant in extrahepatic tissues such as brain, heart, skeletal muscle, and adipose tissue (18). Because heart and skeletal muscle use fatty acids (FAs) as an energy source, and adipose tissue use FAs for energy storage, the VLDL-R is thought to play a role in the delivery of FAs as TG-rich lipoproteins to peripheral tissues (19). The VLDL-R binds with high affinity apolipoprotein E (apoE)-containing particles, such as VLDL and intermediate density lipoprotein from Watanabe heritable hyperlipidemic rabbits, as well as β-VLDL obtained from cholesterol-fed rabbits, but does not bind LDL. In contrast, VLDL from fasted normal human subjects binds with lower affinity than VLDL prepared from Watanabe heritable hyperlipidemic rabbits or β-VLDL from cholesterol-fed rabbits. The low-affinity binding of fasted human VLDL to the VLDL receptor can be overcome by enriching VLDL with either apoE or LPL (18–21). There are three mechanisms between LPL and the VLDL-R: 1) direct binding to the receptor, 2) mediation of the binding lipoprotein particles to heparan sulfate proteoglycans before interaction with the receptor, and 3) its lipolytic activity, converting VLDL particles to smaller remnants (apoE-rich particles) before these can become endocytosed by receptors. After our findings of unique ligand-binding specificity of the VLDL-R for VLDL particles, Niemeier and colleagues (22) showed that the same mechanism was operating for chylomicron particles. The VLDL-R also interacts with numerous other ligands, including LPL (21, 23), urokinase plasminogen activator/plasminogen activator inhibitor-1 complex (23), receptor-associated protein (RAP) (24), and the atherogenic lipoprotein(a) (25). VLDL-R expression, mostly in macrophages, has been demonstrated in human and rabbit atherosclerotic lesions (25–28), and we suggested that the VLDL-R contributes to macrophage foam cell formation in the early phase of atherosclerosis via uptake of remnant lipoproteins (29). Furthermore, we showed a novel VLDL-R pathway for FA metabolism in the heart (30). Taken together, these findings suggest that the VLDL-R plays an important role in lipoprotein metabolism of VLDL and other TG-rich lipoprotein particles in concert with LPL as a peripheral lipoprotein receptor (31).

It has recently been reported that VLDL-R mRNA in skeletal muscle is reduced in experimental hypothyroidism and is increased in hyperthyroidism (32). Reductions of VLDL-R expression have been described in rats with chronic renal insufficiency and nephrotic syndrome and in Imai rats with spontaneous focal glomerulosclerosis (33–35). Rats with these conditions showed marked hypertriglyceridemia, elevated plasma VLDL concentration, and impaired VLDL clearance.

To investigate the role of the VLDL-R in the disorder of lipoprotein metabolism in insulin-deficient diabetes, we studied VLDL-R expression in STZ rats and rat myoblasts (L6 cells).

Materials and Methods

Experimental animals and cultured myoblasts

Adult 8-wk-old male Sprague Dawley (SD) rats (280–310 g) were obtained from Japan SLC (Shizuoka, Japan). Rats were randomly divided into nondiabetes (control) and diabetes (STZ) groups. The animals were made diabetic under halothane anesthesia, followed by injection of STZ (60 mg/kg body weight, iv; Sigma-Aldrich Corp., St. Louis, MO) into the tail vein. An equivalent volume (1 ml/kg) of saline was administered to the nondiabetic controls. Hyperglycemia was tested 24 h after STZ administration by a blood glucose meter. All STZ-treated rats were kept for 1–4 wk after STZ injection, at which time they were killed after 5 h of fasting, and their tissues and plasma samples were collected. All animals were maintained under a 12-h light (0700–1900 h), 12-h dark cycle and given a standard laboratory diet (Oriental Yeast, Tokyo, Japan) and water. All experiments were conducted in accordance with the National Institutes of Health and Welfare Guide for the Care and Use of Laboratory Animals. Rat myoblasts (L6 cells, JCRB9081) were purchased from Health Science Research Resources Bank (Osaka, Japan).

Antibodies against VLDL-R, LDL-R, LDL-R-related protein-1 (LRP1), and glyceraldehyde-3-phosphate dehydrogenase (GAPDH)

Rabbit polyclonal antibody (VR2) to the carboxyl terminus of the VLDL-R was made using a synthetic peptide, CASVGHTYPAISVVSTDDDLA, which is encoded in several tissues and species (29). The specificity of rabbit antibody VR2 was confirmed by immunoblotting against a membrane fraction from ldlA-7 cells (LDL-R-deficient Chinese hamster ovary cells) expressing human type 1 VLDL-R, human LDL-R, and human apoE receptor 2 (data not shown). Hybridoma cells producing a monoclonal antibody against rat LDL-R (IgG 4A4, CRL-1898) and rat LRP1 (IgG 11H4, CRL-1936) were purchased from American Type Culture Collection (Manassas, VA). Anti-GAPDH monoclonal antibody was purchased from Chemicon International (Temecula, CA).

Isolation of membrane fraction from tissues and Western blot analysis

Membrane fractions were prepared according to a standard method (36). Cellular protein was measured using the bicinchoninic acid protein assay kit (Pierce Chemical Co., Rockford, IL). SDS-PAGE was performed on the fractions with 5–20% slab gels containing 0.1% sodium dodecyl sulfate. Total membrane and cell protein (30 μg/lane) for heart, liver, and skeletal muscle were applied and transferred to a polyvinylidene difluoride membrane (Millipore Corp., Bedford, MA) using a Trans-blot (Atto, Tokyo, Japan). Detection of antibodies was performed using a second antibody and was visualized by enhanced chemiluminescence (ECL, Pharmacia Biotech, Uppsala, Sweden).

RNA extraction and Northern blot analysis

Total RNA from heart, liver, and skeletal muscle (soleus muscle) was extracted using the guanidinium thiocyanate method with phenol-chloroform extraction (37). Total RNA (15 μg) was loaded onto a 1% agarose-gel with 9% formaldehyde, which was separated in MOPS [3-(N-morpholino)-propanesulfonic acid] buffer. The RNAs were transferred on to the nylon membrane (GeneScreen Plus, NEN Life Science Products, Boston, MA) by capillary transfer. After UV cross-linking, the membrane was prehybridized and hybridized with cDNA fragments labeled [γ-^{32}P]deoxy-CTP by the random primer method, using Random Primer DNA Labeling kits (Takara Shuzo Co., Ltd., Shiga, Japan). The VLDL-R probe was prepared from digested rat VLDL-R cDNA.

RT-PCR

To analyze isoforms of VLDL-R mRNA, RT-PCR was carried out as previously described (20). cDNA was synthesized from 10 μg total RNA from heart and skeletal muscle, using oligo(deoxythymidine)$_{18}$ primer and SuperScript. One tenth of the cDNA was subjected to PCR with a sense primer (5′-CTAGTCAACAACCTGAATGATG-3′) and an antisense primer (5′-AAGAATGGCCCATGCAGAA-3′). The cDNA was amplified with 250 nM of each primer and 0.75 U *Taq* DNA polymerase in a 50-μl volume of buffer, as recommended by the supplier. The reaction mixture was heated to 94 C for 3 min, followed by 30 cycles of reannealing at 62 C for 1 min, elongation at 72 C for 1 min, and denaturation at 94 C for 1 min. The PCR products were separated by agarose gel electrophoresis and stained with ethidium bromide.

Hepatic VLDL production with Triton WR1339 (TG secretion rate)

On d 28 after saline or STZ treatment, SD (control) and STZ rats were food-deprived overnight. Each rat was injected in the tail vein at 250 mg/kg body weight with a 150 g/liter solution of Triton WR1339 (Sigma-Aldrich Corp.) in 9 g/liter NaCl. Blood samples of 100 μl were drawn before the Triton WR1339 injection and 45, 90, 135, 180, and 360 min later. The plasma TG concentration was measured in each sample as described below. The TG secretion rate was calculated from the increments in the plasma TG concentration per minute, multiplied by plasma volume (estimated as 4% of the body weight). The result was expressed as millimoles per hour per 100 g body weight (38).

Serum measurements

Blood samples were collected from the heart into plane glass tubes after 5 h of food deprivation. After clotting, samples were centrifuged, and serum was collected and stored at −80 C until assayed. Serum glucose, TG, and cholesterol levels were measured with kits (Daiichi Pure Chemicals, Tokyo, Japan). The high-density lipoprotein (HDL) cholesterol concentration was measured after precipitation of apoB-containing lipoprotein with dextran sulfate, phosphotungustate, and magnesium chloride. The VLDL/LDL cholesterol concentration was calculated by subtraction of HDL cholesterol from total cholesterol (TC). Serum insulin was measured with using a commercial kit (SCETI Co., Ltd., Tokyo, Japan). Postheparin plasma was collected 5 min after iv injection of 500 U heparin/kg. Plasma LPL activity was measured using a commercial kit (Progen Biotechnik, Heidelberg, Germany).

Scanning and statistical analysis

The results were scanned and analyzed using the Intelligent Quantifier System (Genomic Solutions, Ann Arbor, MI). Values are presented as the mean ± SD. Statistical analysis was performed using the Mann-Whitney *U* test, and the level of statistical significance was set at $P < 0.05$.

Results

General characteristics and lipid profile

The STZ injection caused a reduction in serum insulin levels that was accompanied by hyperglycemia (Fig. 1, A and B, and Table 1). Body weight gain over 4 wk was reduced in the diabetic rats (STZ rats) compared with the controls (SD rats; 392.5 ± 36.84 *vs.* 253.75 ± 29.73 g; $P < 0.05$). In STZ rats, serum TC and TG concentrations increased gradually, and a progressive rise with time was detected. The TC concentration was 2.5- and 4.2-fold higher than the control values on d 21 and 28, respectively ($P < 0.05$; Fig. 1C). Serum TG levels were also 6.7- and 12.7-fold higher than the controls on d 21 and 28 ($P < 0.05$), respectively (Fig. 1D). The serum VLDL/LDL cholesterol concentration was significantly increased by 5.2-fold on d 28 ($P < 0.05$; Table 1). Agarose-gel electrophoresis showed high concentrations of broad β-migrating lipoproteins in STZ rats on d 28, indicating that high TC and TG concentrations were due to the accumulation of remnant lipoproteins (VLDL remnant and chylomicron remnant). Lane C in Fig 1 shows a human plasma lipoprotein pattern with LDL-sized particles and HDL-sized particles. SD rats contained mainly HDL-sized particles on d 0 and 28, but STZ rats on d 28 contained mainly the remnant lipoproteins (broad β-migrating lipoproteins) that were usually detected in human type III dyslipidemia (Fig. 1E). Serum levels of T_3 in STZ rats showed decreases of 26% on d 28, but these were not statistically significant, and there was no elevation of TSH in STZ rats (Table 1). It was unlikely that severe hyperlipidemia on d 28 was due to hypothyroidism caused by a long-term diabetic state.

Expression of VLDL-R protein in heart and skeletal muscle

The expression of VLDL-R protein in heart tissue showed no change in the control rats, whereas in STZ rats it had decreased to 70% on d 14 and 21 and to 50% on d 28 (Fig. 2, A and C). The expression of VLDL-R protein in skeletal muscle in STZ rats had decreased to 60% on d 3, to 30% on d 14, and to 10% on d 21. On d 28, VLDL-R in skeletal muscle was less than 10% of that in the controls (Fig. 2, B and D). LDL-R protein levels in skeletal muscle showed no consistent changes in control or STZ rats (data not shown).

mRNA levels of VLDL-R in heart and skeletal muscle

In heart tissue, there was little change in the mRNA level of VLDL-R in either STZ or control rats during these periods (Fig. 3A). Also in skeletal muscle, the mRNA level of VLDL-R did not change during the study periods, but it increased on d 7 in control rats and decreased slightly on d 28 in STZ rats (Fig. 3B). It was intriguing that there was a dissociation between VLDL-R protein and mRNA expression in STZ rats. To obtain exact results for VLDL-R mRNA levels in heart and skeletal muscle, we also checked VLDL-R/GAPDH mRNA levels on d 28 by scanning the VLDL-R and GAPDH density. Figure 3C indicates that VLDL-R/GAPDH mRNA levels were decreased by 40% and 24% in heart and skeletal muscle, respectively, but we could not find a statistical significance in the difference between the two groups. Even though we could not clearly indicate the discrepancy between VLDL-R protein and mRNA in heart, it was obvious that the decreased VLDL-R protein level was not related to the VLDL-R mRNA level in skeletal muscle. In contrast, the splice isoform of the VLDL-R mRNA (20) examined by RT-PCR showed no significant difference in the expression of type 1 and type 2 VLDL-R mRNA in heart and skeletal muscle during the study periods (data not shown).

Hepatic TG production rate (TGPR) and postheparin plasma LPL activity

TGPRs were determined after Triton WR1339 injection, which prevents VLDL catabolism and thereby allows TGPR to be calculated. The TGPR during 3 h on d 28 showed no statistically significant difference between control and STZ rats (0.12 ± 0.03 *vs.* 0.10 ± 0.03 mmol/h/100 g body weight). TGPR over 6 h was greater in the controls than in STZ rats (0.13 ± 0.01 *vs.* 0.10 ± 0.02 mmol/h/100 g body weight), although this was not statistically significant (Fig. 4A). There was no difference in VLDL production by liver between the two groups, indicating that the hyperlipidemia in STZ rats on d 28 was not due to VLDL overproduction in liver. In contrast, heparin-releasable plasma LPL activity in STZ rats was reduced early on d 7 compared with the control level, even though there was no significant lipoprotein abnormality between SD and STZ rats (Fig. 1, C and D). On d 21 and 28, severe hyperlipidemia was observed in STZ rats, but the plasma LPL activity level was not changed during the study period (~50% of that in control rats; Fig. 4B). These data